Dissociation of task engagement and arousal effects in auditory cortex and midbrain

Daniela Saderi[1,2], Zachary P. Schwartz [1,2], Charlie R. Heller[1,2], Jacob R. Pennington[3], Stephen V. David[2]

[1]Neuroscience Graduate Program, [2]Oregon Hearing Research Center,

Oregon Health and Science University, [3]Washington State University, Vancouver

Correspondence: SVD, 3181 SW Sam Jackson Park Road, MC L335A, Portland, OR 97239.

Email: davids@ohsu.edu

DS ORCID iD: https://orcid.org/0000-0002-6109-0367

ZPS ORCID iD: https://orcid.org/0000-0002-1854-5450

CRH ORCID iD: https://orcid.org/0000-0002-9048-1201

JRP ORCID iD: https://orcid.org/0000-0001-9393-0474

SVD ORCID iD: https://orcid.org/0000-0003-4135-3104

Keywords: auditory cortex, behavior, pupil, sound

Acknowledgements: This study was supported by NIH grants F31 DC014888 (DS), R01 DC0495 (SVD), and from the Tartar Trust at Oregon Health & Science University (DS).

Abstract

The brain's representation of sound is influenced by multiple aspects of internal behavioral state. Following engagement in an auditory discrimination task, both generalized arousal and task-specific control signals can influence auditory processing. To isolate effects of these state variables on auditory processing, we recorded single-unit activity from primary auditory cortex (A1) and the inferior colliculus (IC) of ferrets as they engaged in a go/no-go tone detection task while simultaneously monitoring arousal via pupillometry. We used a generalized linear model to isolate the contributions of task engagement and arousal on spontaneous and evoked neural activity. Fluctuations in pupil-indexed arousal were correlated with task engagement, but these two variables could be dissociated in most experiments. In both A1 and IC, individual units could be modulated by task and/or arousal, but the two state variables affected independent neural populations. Arousal effects were more prominent in IC, while arousal and engagement effects occurred with about equal frequency in A1. These results indicate that some changes in neural activity attributed to task engagement in previous studies should in fact be attributed to global fluctuations in arousal. Arousal effects also explain some persistent changes in neural activity observed in passive conditions post-behavior. Together, these results indicate a hierarchy in the auditory system, where generalized arousal enhances activity in the midbrain and cortex, while task-specific changes in neural coding become more prominent in cortex.

Introduction

Hearing is a dynamic process that requires integration of the sensory evidence provided by physical attributes of sound with information about the behavioral context in which auditory perception occurs (Bizley and Cohen, 2013; Fritz et al., 2007). As sound information passes through the brain, coordinated activity in auditory areas extracts information necessary to guide behavior. Compared to passive listening, engaging in a task that requires subjects to respond selectively to one or more sounds leads to changes in neurons' excitability, as well as their spectral and spatial selectivity (Downer et al., 2015; Fritz et al., 2005, 2003; Knudsen and Gentner, 2013; Kuchibhotla et al., 2017; Lee and Middlebrooks, 2011; Otazu et al., 2009; Ryan and Miller, 1977; Yin et al., 2014). These changes are often attributed to the current task demands, enhancing the representation of important sound features by increasing or decreasing the activity of specific neural populations (Bagur et al., 2018; David et al., 2012; Kuchibhotla et al., 2017). In some studies, changes have been reported to persist for several minutes after the active behavior, while in others, activity and tuning changes were observed to rapidly return to baseline (Fritz et al., 2003; Slee and David, 2015).

The substantial variability of effects across studies suggests that task-related modulation is produced by multiple non-auditory signals, reflecting a complex internal state. Changes in the activity of auditory neurons have been attributed to temporal expectation (Jaramillo and Zador, 2011), reward associations (Beaton and Miller, 1975; David et al., 2012), self-generated sound (Eliades and Wang, 2008), and non-sound related variables, such as motor planning (Bizley et al., 2013; Huang et al., 2019) and decision-making (Tsunada et al., 2015). Even in the absence of external sensory input, fluctuations are observed in neural activity throughout the forebrain, including primary sensory regions (Ringach, 2009; Stringer et al., 2019). This activity is related

65 to cognitive states such as arousal, and might be acting to boost responses to sensory stimuli
66 relevant to the current task demands (Fu et al., 2014; Wimmer et al., 2015). Therefore,
67 attempting to interpret changes in neuronal activity solely in the light of a single state variable,
68 such as task engagement, may lead to an incomplete and sometimes incorrect understanding of
69 how sensory information is processed under conditions that necessarily engage multiple aspects
70 of cognition.

71 A straightforward and non-invasive way to measure one aspect of behavioral state is by
72 monitoring non-luminance-mediated changes in pupil size (Kahneman and Beatty, 1966;
73 McGinley et al., 2015; Zekveld et al., 2018). In humans, changes in pupil size under constant
74 light exposure have been shown to correlate with mental effort (Beatty, 1982; Winn et al., 2015),
75 changes in states of arousal (Kahneman and Beatty, 1966), aspects of decision-making (Gilzenrat
76 et al., 2010), and task performance (Schriver et al., 2018). Fluctuations in pupil size also closely
77 track locomotion and neural activity throughout the mouse forebrain (McGinley et al., 2015;
78 Stringer et al., 2019). Thus, pupil size can be easily measured simultaneous to neuronal activity
79 and used to account for effects of arousal on sound-evoked activity.

80 To study the interaction of task engagement and arousal on auditory neural coding, we
81 recorded extracellular spiking activity and pupil size of ferrets during an auditory task and during
82 passive presentation of task stimuli. Single- and multiunit activity was recorded from the primary
83 auditory cortex (A1) and midbrain inferior colliculus (IC). We used a generalized linear model to
84 quantify the unique contributions of pupil-indexed arousal and task engagement to neural
85 activity. Using this approach, we found that subpopulations of recorded neurons were modulated
86 uniquely by task or by arousal, suggesting that these effects are mediated by distinct modulatory
87 circuits. The modeling analysis also revealed that in many neurons, arousal state could account

for variability in firing rate that might otherwise be attributed to task engagement. This result suggests that some previously reported effects of task engagement may in fact be explained by changes in pupil-indexed arousal. In addition, the relative effects of arousal and task engagement varied between cortex and midbrain. Pupil-related changes occurred in both areas, but task engagement effects were more prominent in A1. This work highlights the value of accounting for multiple state variables in studies of sensory coding (Musall et al., 2019; Stringer et al., 2019), both in identifying the source of task-related effects and locating where in the sensory processing hierarchy they emerge.

Results

Changes in pupil size track task engagement

To study interactions between arousal and task engagement, we trained four adult ferrets on a go/no-go auditory detection task (David et al., 2012; Yin et al., 2010). Animals reported the presence of a target tone following a random number of broadband noise reference stimuli (Figure 1A, B). They were required to withhold licking a water spout during the reference sounds and were given liquid reward for licking during the target window (100-1500 ms after target onset). Targets were pure tones, either presented alone (tone versus noise discrimination, Ferret L) or embedded in reference stimuli (tone-in-noise detection, Ferrets R, B, and T). After training, all animals performed consistently above chance (Figure 1C).

To track and record changes in pupil size, an infrared video camera was used to image the eye contralateral to the speaker emitting auditory stimuli (Figure 1A). Constant luminance was maintained throughout the experiment so that fluctuations in pupil size reflected only changes in internal state (McGinley et al., 2015; Schwartz et al., 2020). Pupil was recorded continuously as animals passively listened to the task stimuli and actively performed the task. The distribution of pupil size differed between passive and active conditions (Figure S1A). Mean pupil diameter was consistently larger during active behavior ($p = 1.6 \times 10^{-6}$, sign test, Figure 1D). Within active blocks, pupil size also varied with task performance. Average pupil size was similar for false alarm and hit trials, but it was smaller during miss trials, more closely resembling passive trials (Figure S1B). In addition, the short-term dynamics of pupil displayed a strong dependence on task condition. During behavior, trial onset evoked a rapid increase in pupil size, which was absent during passive listening ($p = 5.6 \times 10^{-8}$, sign test, Figure 1E-F).

Thus, pupil size tracked slow changes in task-engagement (active versus passive blocks) as well as more rapid changes in trial-by-trial performance during the active condition.

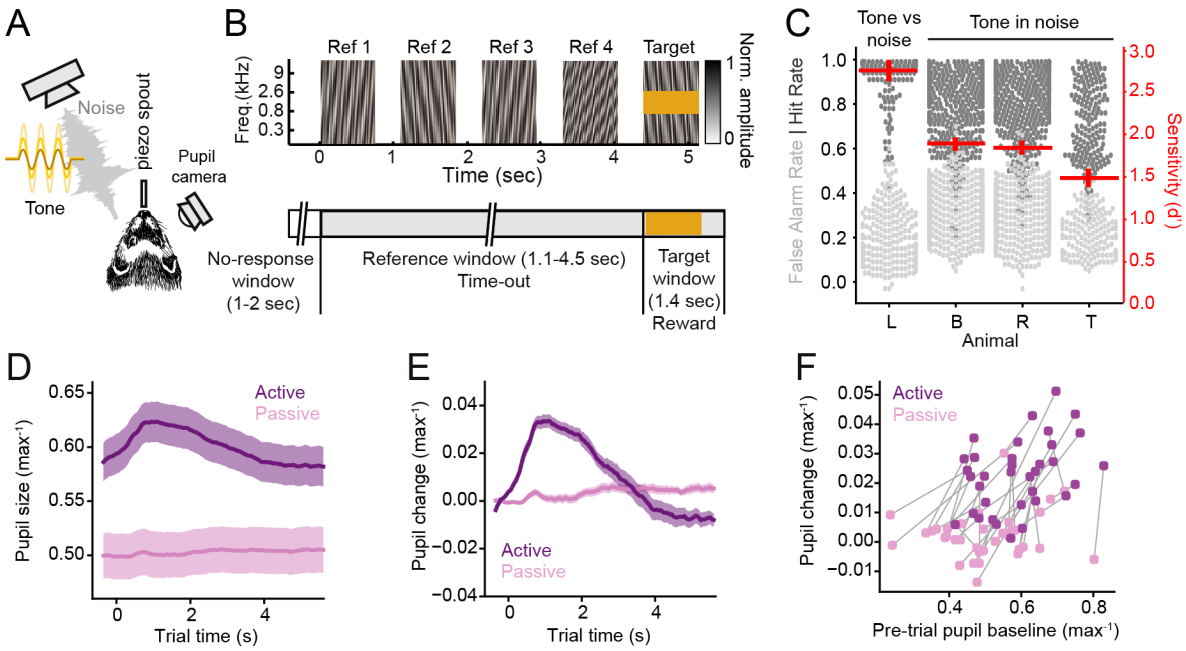

Figure 1: Pupil size correlates with task engagement. **A.** Schematic of behavioral setup, including free-field speaker for sound presentation, piezo spout to register licks and deliver reward, and infrared video camera for pupillometry**. B.** Spectrogram of example trial (top) and task structure (bottom). False alarms before the target window were punished with a timeout and hits resulted in a liquid reward. **C.** Swarm plot showing behavioral performance (hit rate or false alarm rate) for each animal. Each point corresponds to a behavioral block. Red lines indicate mean and standard error of the mean (SEM) of the sensitivity (*d*') for each animal. All animals performed above chance on average (*d*' > 1). **D.** Mean timecourse of pupil size aligned to trial onset for active and passive blocks, averaged across all animals and sessions and normalized to maximum size per session. Shading indicates SEM. **E.** Average timecourse of change in pupil size, normalized to 0.35-s pre-trial period for active and passive behavioral blocks. **F.** Scatter plot compares pre-trial pupil size and mean change per trial (3-s post-onset window). Each dot represents a behavioral block. Passive and active blocks within the same session are connected by a line.

Distinct task engagement and arousal effects in A1 and IC neurons

We recorded extracellular spiking activity from the primary auditory cortex (A1, n = 129 units) and the inferior colliculus (IC, n = 66 units) of ferrets, while they switched between active engagement and passive listening. In the IC, we recorded from central (ICC, n = 18 units) and

141 non-central regions (NCIC, n = 48 units), distinguished by their functional topography (Slee and
142 David, 2015). Results from the IC are presented jointly between the two sub-regions, unless
143 otherwise specified.

144 To study how behavior state modulated auditory neural activity over time, we recorded
145 activity in the same units over multiple passive and active blocks and recorded pupil diameter
146 throughout each experiment. For analysis, the peri-stimulus time histogram (PSTH) response to
147 the reference stimuli was averaged across passive and correct (hit) active trials, and data from
148 target periods were excluded. On hit trials, animals did not lick during the reference stimuli; thus
149 this approach reduced the possibility that lick-related motor signals confounded our results
150 (Brosch et al., 2005; Schneider et al., 2014; Stringer et al., 2019).

151 For many units, activity appeared to be modulated by changes in task engagement, as
152 would be expected from previous behavioral studies (Fritz et al., 2003; Kuchibhotla et al., 2017;
153 Niwa et al., 2012; Otazu et al., 2009). During active behavior, responses to the noise stimuli
154 either increased or decreased, and then returned to their baseline passive state during subsequent
155 passive periods (Figure 2A-B). For other units, however, no consistent change in activity was
156 observed between active and passive conditions. In these cases, firing rate could change between
157 behavioral blocks, but the effect was not consistent across engagement conditions (Figure 2D-E).
158 Thus, despite our controls for sound acoustics and motor activity, the firing rates of some units
159 varied over time in a way that did not appear to be related to task engagement.

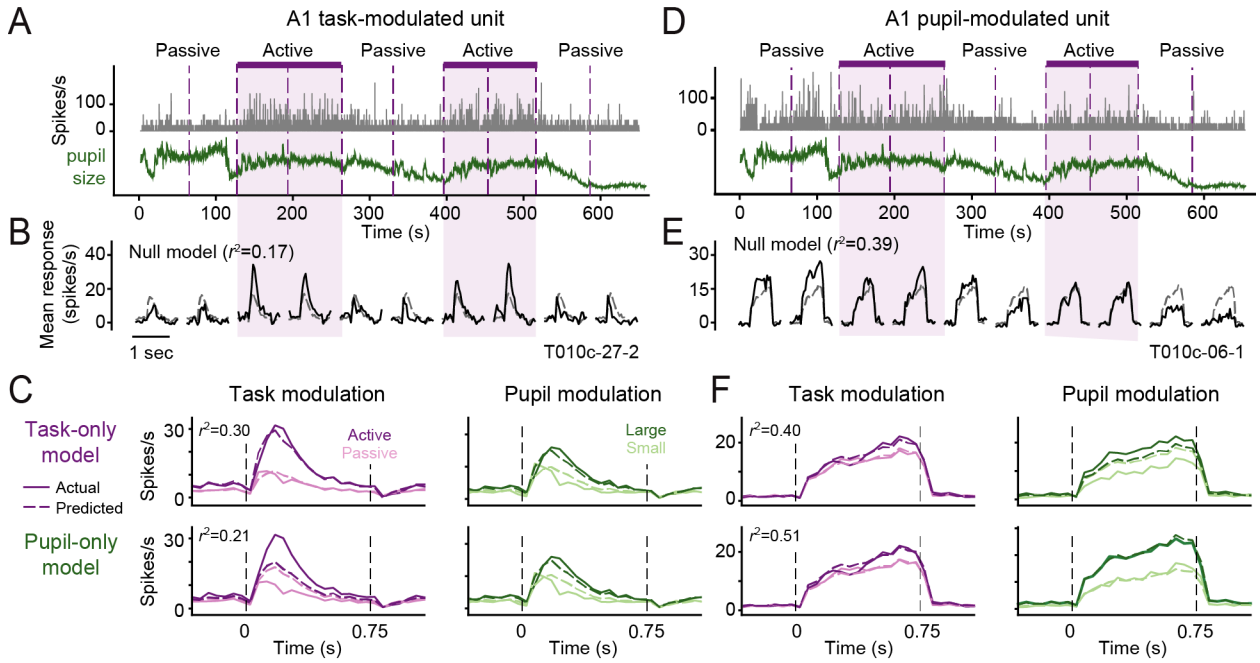

Figure 2: Simultaneously recorded units showing task versus pupil-related changes. **A.** Firing rate (grey) of one neuron during the reference period and time-aligned pupil size (green) over the duration of one experiment (total recording time ~1h, inter-trial and target periods not shown). Purple shading highlights active blocks. Dashed lines delineate boundaries between half of each behavioral block. **B.** Peristimulus time histogram (PSTH) responses to reference noise averaged across each half block (black). Dashed gray lines are responses predicted by the null model, i.e., the PSTH averaged across all blocks. Model prediction accuracy is indicated by fraction variance explained (r^2). **C.** Top: PSTH response for the example unit averaged across passive and active blocks (left) and averaged across large- and small pupil trials (right). Predictions of the task-only model are overlaid (dashed lines). Modulation index (*MI*) measures the fraction change in predicted response between two behavior conditions (MI_{AP} *task-only* = 0.36, MI_{LS} *task-only* = 0.17). Bottom: Active/passive and large/small responses plotted with predictions by the pupil-only model, which only accounts for pupil-related changes (MI_{AP} *pupil-only* = 0.062, MI_{LS} *pupil-only* = 0.17). **D.** Firing rate and pupillometry for a second unit, recorded simultaneously to the first example. **E-F.** PSTH responses for the second unit, plotted as in B-C. The task-only model does not capture pupil-related changes (MI_{AP} *task-only* = 0.067, MI_{LS} *task-only* = 0.029). The pupil-only model captures both task- and pupil-related changes (MI_{AP} *pupil-only* = 0.10, MI_{LS} *pupil-only* = 0.26).

We wondered if changes in activity that could not be attributed to task engagement could instead be explained by fluctuations in pupil-indexed arousal (Lin et al., 2019; McGinley et al., 2015; Schwartz et al., 2020). A simple way to investigate if arousal affects firing rates is to divide all trials (both active and passive) into two groups, based on the mean pupil size during each trial, and compute a separate PSTH for each group (Figure 2C, F). One group was made for

185 trials with pupil size smaller than the median computed across the entire experiment, and the
186 other for trials with pupil size larger than the median. This analysis showed that activity was
187 often enhanced when pupil was large (large versus small pupil PSTH, Figure 2C, F), indicating
188 that pupil size was positively correlated with firing rate.

189 Because changes in pupil size were correlated with transitions between active and passive
190 blocks (Figure 1E), we could not dissociate the effects of task engagement and arousal using just
191 the raw PSTH. Therefore, to test our hypothesis that pupil accounted for changes in neural
192 activity following task engagement, we fit a generalized linear model (*Eqn. 1*) in which the
193 response baseline and gain for each presentation of the reference stimuli was modulated by task
194 engagement and pupil size. Task engagement was modeled as a discrete regressor (active or
195 passive) and pupil as a continuous regressor. In some datasets, we changed task conditions
196 between active blocks by varying the SNR or the target tone frequency. In these cases, we
197 included a separate regressor for each condition to account for possible task-specific changes in
198 activity (Figures S4, S5). This approach allowed us to dissociate effects of arousal and task
199 engagement on firing rate.

200 Model performance was measured by the fraction variance explained (squared correlation
201 coefficient, r^2) between the predicted and actual single-trial spike rates, using 20-fold cross
202 validation. To test for significant contributions of each regressor, we introduced these variables
203 stepwise (Fritz et al., 2010; Musall et al., 2019). The full model included both pupil and task
204 engagement variables. We compared performance of the full model to the performance of a
205 state-independent model, for which both pupil and task variables were shuffled in time (null
206 model), and of two partial models, which accounted for effects of a single state variable while
207 shuffling the values of the other variable in time (pupil or task partial models).

The regression analysis revealed that that some units were driven more by task engagement and others by pupil-indexed arousal. For some units, the modulation of firing rate between active and passive blocks was almost completely accounted for by the task variable, with little contribution of pupil-indexed arousal (example in Figure 2A-C). The null model was not able to account for variability between behavior blocks ($r^2 = 0.12$, Figure 2B, dashed lines). When we added the task variable, predictions significantly improved with respect to the null model (task partial model, $r^2 = 0.30$; jackknifed *t*-test, $p < 0.05$; Figure 2C). Pupil size was also able to account for some changes in firing rate (pupil partial model, $r^2 = 0.21$), but the full model incorporating both task engagement and pupil showed no additional improvement over the task partial model ($r^2 = 0.30$). Thus, all behavior-dependent changes for this unit were accounted for by task engagement. The apparent pupil effects were in fact explained by correlations between pupil size and task engagement.

Conversely, for other units, changes in firing rate were uniquely accounted for by arousal (example in Figure 2D-F). For these units, the task partial model ($r^2 = 0.39$) might indicate a small improvement over the null model ($r^2 = 0.40$, $p > 0.05$, jackknifed *t*-test, Figure 2F). However, the pupil partial model showed a significant improvement over the null model and was able to account for changes in the PSTH between passive and active ($r^2 = 0.51$, $p < 0.05$). The full model showed no additional improvement over the pupil partial model ($r^2 = 0.53$, $p > 0.05$). Thus, we found evidence for A1 units whose activity could be modulated either by task or by arousal.

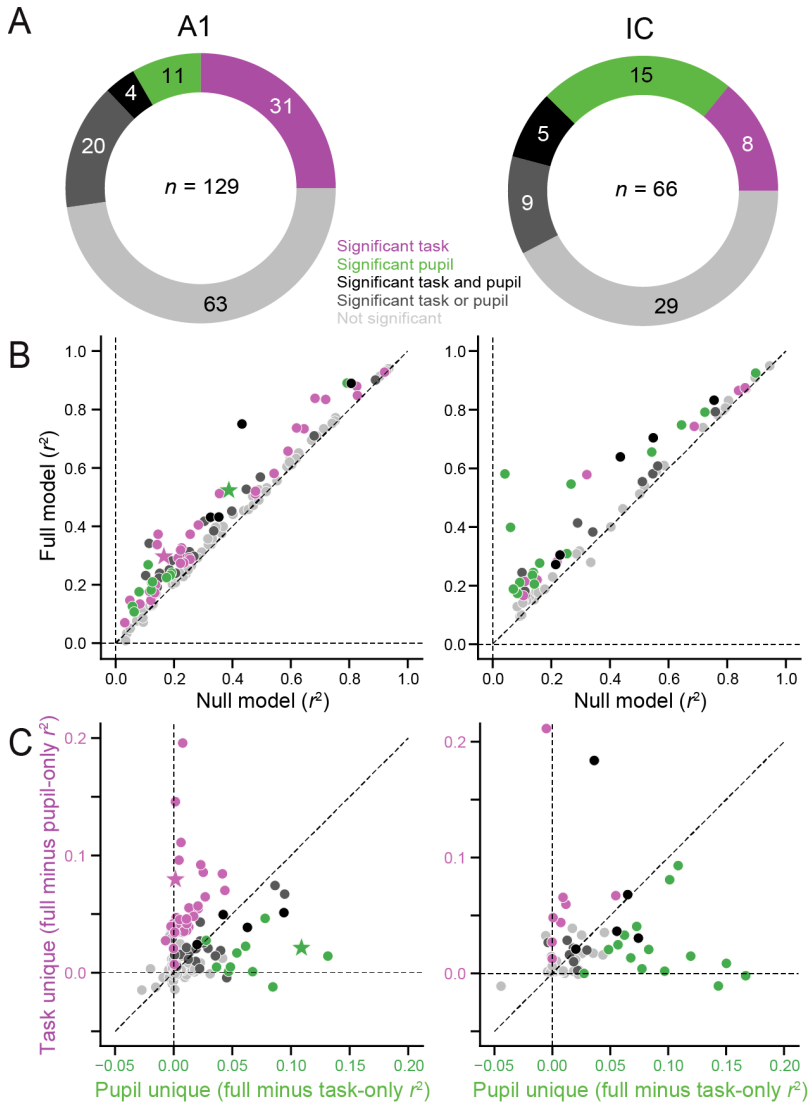

Figure 3: Task and pupil-related modulation of firing rates in A1 and IC. **A.** Doughnut plots indicate number of units significantly modulated by task, arousal, or both in A1 (left) and IC (right, $p < 0.05$, jackknifed t-test). Total number of recorded units reported in the center. Purple and green: significant unique modulation of task or pupil, respectively. Black: both unique task and pupil contributions. Dark grey: ambiguous task or pupil modulation. Light gray: no significant change in accuracy between full and null models. **B.** Scatter plot of variance explained (r^2) in single-trial activity by full model versus null model. Each symbol represents a unit in AC (left) or IC (right). Colors as in A. **C.** Unique variance explained by pupil size plotted against unique variance explained by task engagement for each unit. Stars correspond to examples in Figure 2A (purple) and D (green).

Next, we investigated the prevalence of task- and arousal-related modulation across the population of A1 and IC units. To quantify the relative contribution of each variable to model performance, we compared the variance in single-trial spike rate explained by each of the four

243 models (r^2). Across the entire dataset, 66/129 (51%) A1 units and 37/66 (56%) IC units showed a
244 significant increase in r^2 for the full model over the null model, indicating an effect of either
245 engagement or pupil ($p < 0.05$, jackknife *t*-test; Figure 3A). By computing the difference
246 between the cross-validated r^2 for the full model and for the two partial models separately, we
247 determined the variance that could be uniquely explained by either arousal or task in each unit.
248 This produced four categories of state-modulated neuron (Figure 3A): units for which both task
249 and pupil uniquely contributed to the modulation (black); units for which only one variable, task
250 (purple, *e.g.*, Figure 2A) or pupil (green, Figure 2D), contributed uniquely; and units for which
251 showed behavior changes that could not be uniquely attributed to task or pupil (dark gray).
252 A comparison of variance explained across the entire dataset shows consistent
253 improvement by the full model over the null model in both A1 (mean r^2 null: 0.282, full: 0.340, p
254 $= 6.37 \times 10^{-23}$, Wilcoxon sign test) and IC (mean r^2 null: 0.290, full: 0.399, $p = 6.77 \times 10^{-15}$,
255 Figure 3B). Although the proportion of units with any significant state-related modulation was
256 comparable between A1 and IC, only about a quarter of those A1 units showed unique pupil-
257 dependent modulation (15/66), compared to about a half for IC (20/37). The average variance
258 uniquely explained by each state variable also differed between areas. In A1, the variance
259 explained by task (mean r^2 task unique: 0.017) was significantly greater than variance explained
260 by pupil (mean r^2 pupil unique: 0.007, $p = 0.00201$, Wilcoxon sign test, Figure 3C). In IC, the
261 variance explained was not significantly different between task and pupil (mean r^2 task unique:
262 0.016, mean r^2 pupil unique: 0.018, $p = 0.236$). Thus, while both the magnitude and prevalence
263 of state-dependent modulation in A1 was more pronounced for task than for pupil, modulation in
264 the IC was equally shared between the two variables.

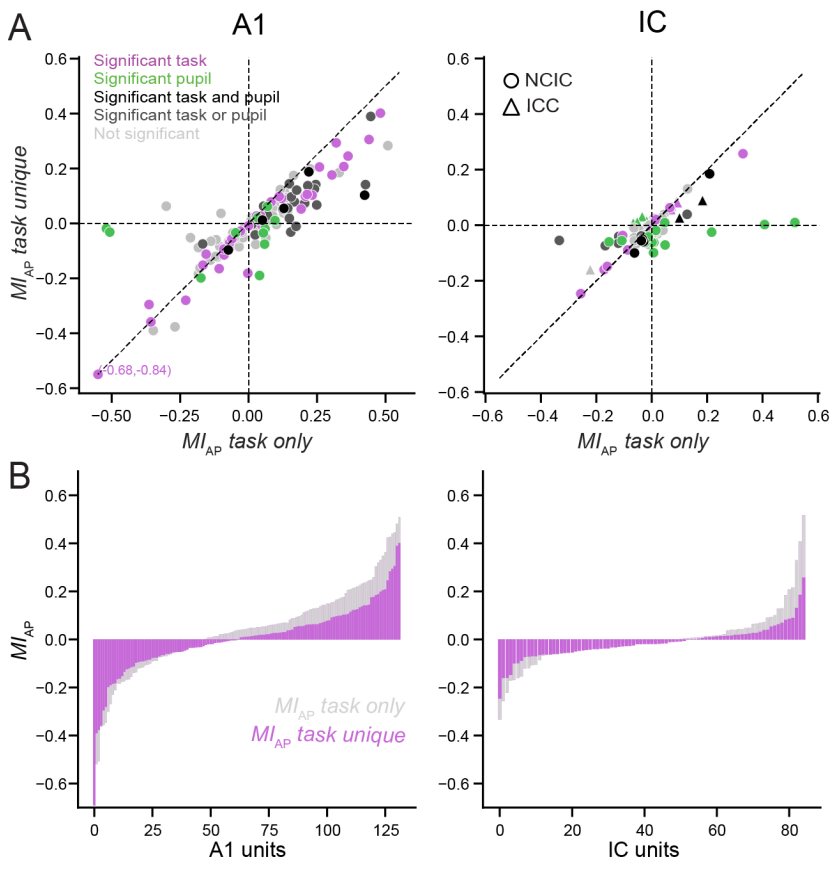

Figure 4: Changes in arousal account for apparent task engagement effects. **A.** Active versus passive modulation index computed from responses predicted by the task only model (MI_{AP} *task-only*), in which pupil is shuffled, plotted against MI_{AP} *task-unique*, in which pupil-dependent modulation is regressed out, for A1 (left, n = 132 unit/target pairs) and IC (right; circles for NCIC, n = 24, triangles for ICC units, n = 61). Colors indicate significant unique variance explained by one or two state variables, as in Figure 3 ($p < 0.05$, jackknife t-test). **B.** Overlaid histograms of MI_{AP} *task-only* and MI_{AP} *task-unique*, sorted according to their magnitude for each unit in A1 and IC. Accounting for pupil-indexed arousal reduces the magnitude of MI_{AP} by about 33% in both areas (A1: $p = 6.78 \times 10^{-10}$; IC: $p = 0.041$; sign test).

Pupil-indexed arousal accounts for apparent task engagement effects in both A1 and IC

So far, we have shown that a significant number of units in A1 and IC show state-dependent modulation of activity, with a large portion exhibiting pupil-dependent modulation. Furthermore, the observation that pupil size is correlated with task engagement (Figure 1) suggests previous characterizations of task-related plasticity that did not measure pupil might have attributed arousal related changes to task engagement (Downer et al., 2015; Fritz et al.,

2003; Knudsen and Gentner, 2013; Kuchibhotla et al., 2017; Lee and Middlebrooks, 2011; Otazu et al., 2009; Ryan and Miller, 1977; Yin et al., 2014). Therefore, we asked to what extent arousal-related modulation could explain changes in activity between active and passive blocks that would otherwise be attributed to task alone.

To quantify the magnitude and sign of the modulation by task engagement, we used a modulation index (*MI*), which measured the fraction change in mean predicted firing rate between active and passive conditions (*Eqn. 5*, see *Materials and Methods*) (Otazu et al., 2009; Schwartz and David, 2018). By computing *MI* from model predictions, we could isolate the unique effects of the state variables, using the same logic as for the unique variance explained calculation (above, Figure 3C). If one ignored pupil, *MI* was computed from predictions of the task only model (MI_{AP} *task-only*). To account for effects of both task and pupil, *MI* was computed from predictions by the full model (MI_{AP} *full*). Finally, modulation that could be explained by arousal was computed using the pupil-only model (MI_{AP} *pupil-only*). Then the unique task-related change, MI_{AP} *task-unique*, was computed as the difference between MI_{AP} *full* and MI_{AP} *pupil-only*.

A comparison of MI_{AP} *task-only* and MI_{AP} *task-unique* shows that a task-only model often overestimates the magnitude of changes due to task engagement (Figure 4A). To measure the magnitude of this effect across the population, we normalized the sign of MI for each unit so that the mean of MI_{AP} *task-only* and MI_{AP} *task-unique* was always positive. This normalization accounted for the bidirectionality of modulation while avoiding bias that would result from normalizing sign for just a single condition. After sign normalization, accounting for arousal led to a significant decrease *MI* magnitude across units in both A1 and IC (A1: $p = 6.78 \times 10^{-10}$; IC: $p = 0.041$; sign test). Effectively, accounting for pupil led to a 33% reduction in the magnitude of

305 MI_{AP} in both A1 and IC (A1: median MI_{AP} *task-only* magnitude = 0.141; MI_{AP} *task-unique* =
306 0.095; IC: median MI_{AP} *task-only* magnitude = 0.069; MI_{AP} *task-unique* = 0.046). The effect of
307 removing pupil-related activity on the magnitude of active versus passive modulation was also
308 not different between central and non-central regions of IC (ICC versus NCIC, rank-sum test,
309 statistic = -1.386, $p = 0.166$, Figure S2). Taken together these results show that arousal
310 accounted for a significant portion of the change in activity between passive and active blocks in
311 A1 and both regions of IC.
312

313 **Task-related modulation is bidirectional in A1 and mostly suppressive in IC**

314 Previous studies have reported either positive (David et al., 2012; Fritz et al., 2003; Yin
315 et al., 2014) or negative (Otazu et al., 2009; Slee and David, 2015) changes in spike rate
316 associated with task engagement. Variability in task-dependent changes in auditory cortex has
317 been explained by differences in neural selectivity for task stimuli (Fritz et al., 2003), task
318 structure (David et al., 2012), behavioral effort (Atiani et al., 2009), and selective attention
319 (Schwartz and David, 2018). Given that we used a positive reinforcement structure similar to
320 previous studies, we expected the average sign of task-related modulation to be positive in A1
321 (David et al., 2012) and negative in IC (Slee and David, 2015). However, after accounting for
322 effects of pupil in A1, we found that *MI* was equally likely to be positive or negative (40/69
323 positive, median MI_{AP} *task-unique* = 0.018; sign test, statistic = 929.0, $p = 0.0959$; Figure 4B). In
324 contrast, the average effects of increased pupil size was positive in A1 (55/69 positive, median
325 MI_{LS} *pupil-unique* = 0.038; sign test, statistic = 929.0, $p = 3.29 \times 10^{-5}$; Figure 5). Since task
326 engagement is correlated with a larger pupil, firing rates do tend to increase during behavior.

However, this increase can be attributed to increased arousal rather than engagement in the specific task.

In IC, results were consistent with previous reports. Firing rates decreased on average during task engagement (17/49 positive, median MI_{AP} *task-unique* = -0.022; sign test, statistic = 347.0, p = 0.00827). This decrease was significantly different from the average change in A1 (p = 0.00658, Wilcoxon rank-sum test). As in A1, firing rates increased with large pupil (31/49 positive, median MI_{LS} *pupil-unique* = 0.022; sign test, statistic = 929.0, p = 0.010; Figure 5). Thus in the case of IC, accounting for effects of pupil unmasked an even stronger overall decrease in spike rate during task engagement. Most state-related effects were similar in ICC and NCIC. In this case, however, the negative task-related modulation was only observed in NCIC (median MI_{AP} *task-unique* ICC: 0.012, p = 0.0869, NCIC: -0.049, $p = 7.31 \times 10^{-4}$, Figure S2).

Some previous work has also reported that the effect of task engagement can depend on the relationship between task-relevant sound features and the receptive field of individual neurons. During a tone detection task, response gain in IC is selectively suppressed for neurons with best frequency near the target tone frequency (Slee and David, 2015). In A1, frequency tuning is suppressed at the target frequency, despite there being no systematic difference in overall response gain between neurons with best frequency near or far from the target (David et al., 2012). We observed the same pattern of suppression at the target frequency during behavior in the current dataset, even after accounting for arousal effects (Figure S3). We also considered whether state-dependent effects varied with task difficulty but found no differences between pure tone, high SNR tone-in-noise (easy), and low SNR tone-in-noise (hard) conditions (Figure S4).

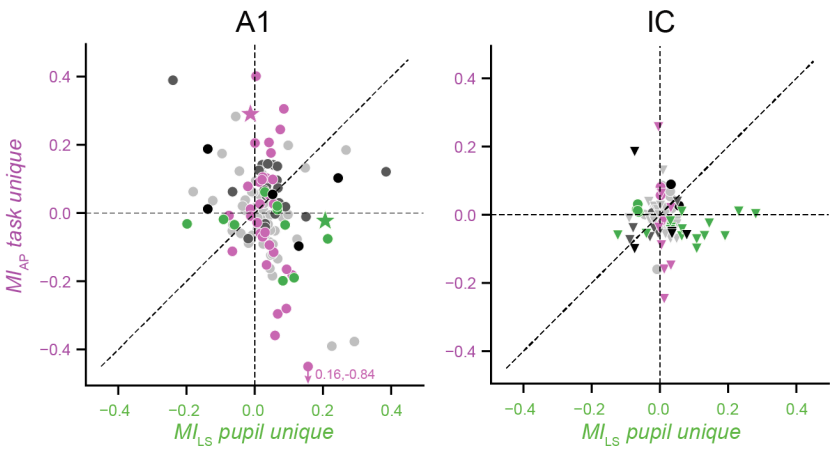

Figure 5: Unique task and arousal modulations are uncorrelated. Scatter plot compares firing rate modulation attributed to task engagement (*MI_{AP} task-unique*) against modulation attributed to pupil (*MI_{LS} pupil-unique*) for each unit in A1 (left) and IC (right). The two quantities showed a weak negative correlation in A1 (r = -0.281, p = 0.00112) and were uncorrelated in IC (r = -0.104, p = 0.343). Colors indicate relative model performance as in Figure 3, and stars indicate examples from Figure 2.

Task engagement and arousal modulate independent neural populations

In some neurons, the effects of task engagement and arousal on firing rates are difficult to dissociate by simply looking at raw activity (*e.g.*, Figure 2D). The regression analysis above disambiguated the unique contribution of each state variable to firing rate modulation. This analysis showed that often only one state variable, task or arousal, modulated the activity of individual units. Based on this observation, we wondered if arousal and task operated via functionally distinct or common pathways. While identifying specific anatomical circuits was outside the scope of this work, we reasoned that if the two modulations were mediated by the same inputs to A1 and IC, a unit modulated by task engagement would also tend to be modulated by arousal. To test this prediction, we measured Pearson's correlation between *MI_{AP} task-unique* and *MI_{LS} pupil-unique* (Figure 5). The latter measure quantified the difference in activity between large and small pupil after regressing out possible task engagement effects (*Eqn. 7*). We found a significant negative correlation between these quantities in A1 (r = -0.281, p = 0.00112)

and no correlation in IC (r = 0.104, p = 0.343). The absence of a positive correlation between task and arousal effects suggests that independent populations of neurons are in A1 and IC are modulated by these variables. To test directly for dependence between task and pupil effects, we performed a permutation test, estimating the number of units that would show both task- and pupil-unique effects if the likelihood of these effects was independent ($p < 0.05$, jackknife t-test, counts from Figure 3). The frequency of joint occurrences was no greater than expected for independent distributions in both areas (A1: p = 0.41, IC: p = 0.59). This independence is consistent with the hypothesis that separate neural circuits mediate task and pupil effects.

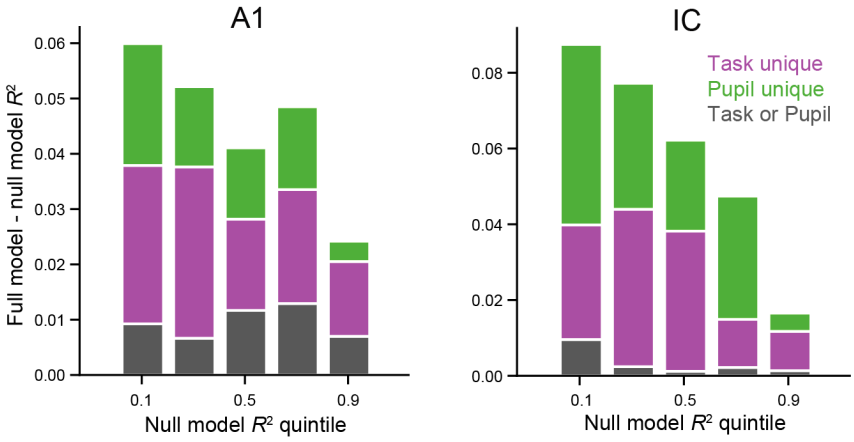

Figure 6: Task and arousal-related modulation in A1 and IC. Mean variance in firing rate explained by behavioral state variables, broken down by effects attributed to task (purple), attributed to pupil (green), and not uniquely attributable to either state variable (grey) for A1 (left) and IC (right). Data are grouped in quintiles by r^2 for the null model performance, a measure of auditory responsiveness. Variance explained by state was not correlated with null model performance in A1 (r = -0.134, p = 0.123), but these values were negatively correlated in IC (r = -0.323, p = 0.00254). Colors as in Figure 4.

Relationship between state modulation and auditory responsiveness

While all units were recorded from areas functionally and anatomically characterized as auditory, neurons within a single auditory field can vary substantially in their tendency to respond to sound (Atiani et al., 2014; Gruters and Groh, 2012). We noticed that some units,

391 particularly in IC, did not show strong auditory responses but were modulated during behavior
392 (*e.g.*, Figure 7B). We asked whether the magnitude of the state-dependent modulation in each
393 recorded unit was related to how reliably it responded to repeated presentations of the same
394 auditory stimulus. Auditory responsiveness was quantified by the variance explained by the null
395 model, since it described how accurately the PSTH response to the reference stimuli, averaged
396 across the entire recording, predicted responses on single trials. Larger or smaller values of null
397 model r^2 were associated with units whose auditory responses were, respectively, more or less
398 reliable across the experiment. We compared this measure of auditory responsiveness to the
399 change in r^2 between the full and null models, which indicates additional variance explained by
400 the state variables. In IC, but not in A1, units that responded less reliably to sound also showed
401 greater dependence on state (A1: r = -0.134, p = 0.123; IC: r = -0.323, p = 0.00254; Figure 6,
402 Figure S5A).

403 High prediction accuracy by the null model limits the variance that can be explained by
404 behavioral state (note relatively weak state effect in highest quintile in Figure 6. We performed a
405 similar analysis but measured the correlation between null model performance and the fraction of
406 remaining variance explained by pupil and task. In this case, null model performance was
407 positively correlated with the remaining variance explained in A1 (r = 0.301, p = 4.61 x 10^{-4})
408 and not correlated in IC (r = 0.124, p = 0.258, Figure S5A). These relationships were also
409 observed when auditory responsiveness was defined as the signal-to-noise ratio of the spectro-
410 temporal receptive field (STRF) measured during passive listening (Figure S5B) (Klein et al.,
411 2000). The same results also held true for a larger pool of neurons, which included data collected
412 without pupillometry and were analyzed with the task-only model (Figure S5C). Thus, while

state-dependent modulation in A1 did not depend on sensory responsiveness, in IC effects of behavioral state were more common in units with a weaker sensory response.

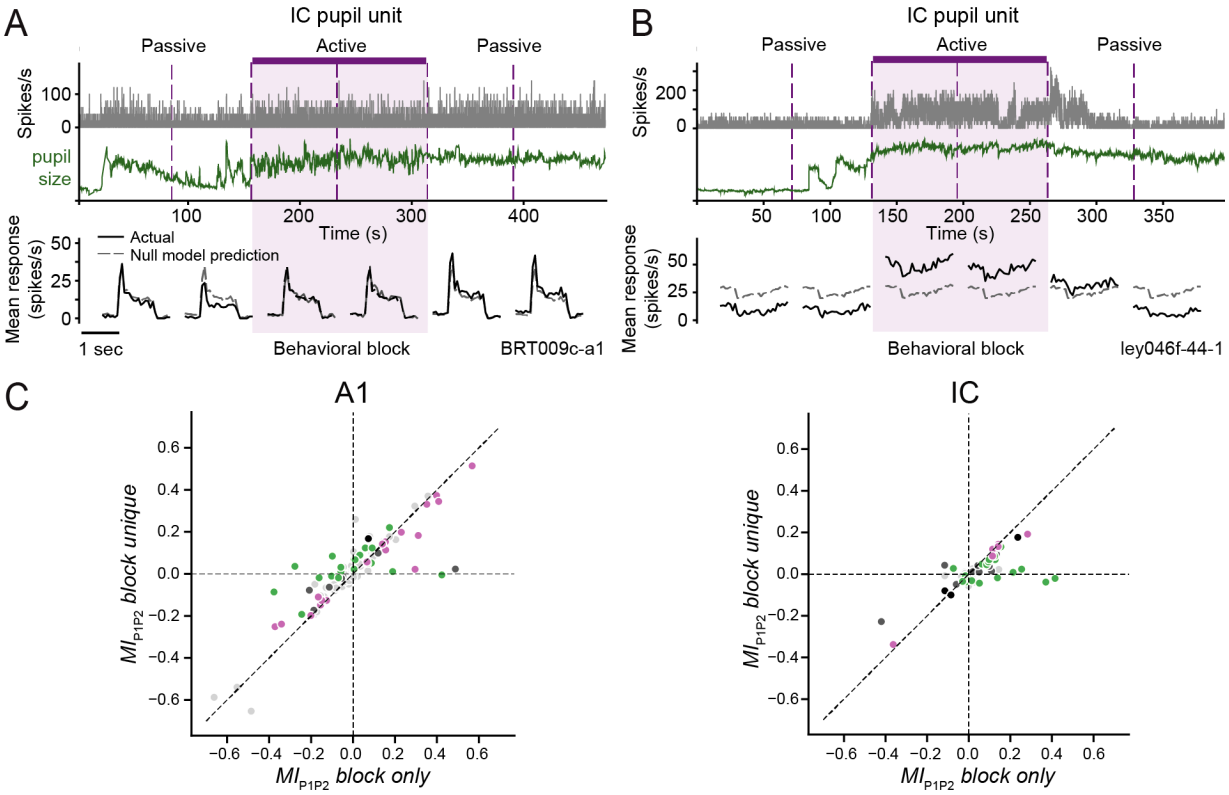

Figure 7: Arousal explains some persistent task-related modulation. **A.** Top: activity of ICC unit and concurrent pupil size recorded over passive and active blocks, plotted as in Figure 2. Bottom: PSTH response to reference noise averaged over each half block (black) with null model prediction overlaid (dashed gray). The response was enhanced slightly during the post-passive (P2) block relative to pre-passive (P1). Without accounting for effects of pupil, this suggests a sustained firing rate increase after behavior, MI_{P1P2} *block-only* = 0.25. After accounting for changes in pupil, the task-related effect is reduced, MI_{P1P2} *block-unique* = 0.02. **B.** Data from example NCIC unit, plotted as in A. The PSTH shows a weak, suppressive response to the reference stimuli, but a large increase in mean firing rate that persists into the first half of the post-passive block (MI_{P1P2} *block-only* = 0.37). Again, the persistent change in firing rate can be accounted for by the very large pupil during the first half of P2 (MI_{P1P2} *block-unique* = -0.04). **C.** Scatter plot compares MI_{P1P2} *block-only* and MI_{P1P2} *block-unique* for A1 (left) and IC (right). Colors as in Figure 4. Accounting for pupil reduces *MI* attributed to persistent effects after behavior in both areas (A1: $p = 0.00120$, IC: $p = 9.39 \times 10^{-6}$, Wilcoxon signed-rank test).

Changes in arousal explain some persistent post-behavior state effects

Previous studies in both A1 (Fritz et al., 2003) and IC (Slee and David, 2015) have reported examples of task-related modulation persisting in passive blocks following active engagement (referred to as post-passive blocks). These effects have been interpreted as persistent task-related plasticity, but they are highly variable and difficult to attribute to any specific aspect of the behavior. We observed these effects in our data as well. In addition to units in A1 (*e.g.*, Figure 2D), some units in IC showed persistent changes in activity during passive blocks following behavior. These changes sometimes lasted through the entire post-passive block (Figure 7A) and other times gradually reverted to pre-passive levels (Figure 7B). The timecourse of these changes often tracked fluctuations in pupil size.

To measure the presence of persistent task-related modulation – and the extent to which arousal accounts for it – we compared the activity between passive blocks before (P1) and after (P2) a behavior block. We performed a regression analysis similar to that used for measuring task engagement effects, but treating passive block identity (P1 or P2) as a state variable in addition to pupil. Modulation index was computed for predictions by a model based only on block identity, ignoring pupil (MI_{P1P2} *block-only*), and for the unique contribution of passive block after accounting for pupil effects (MI_{P1P2} *block-unique*, Figure 7A). We assessed the magnitude of *MI* using the same sign normalization as for the task-unique *MI* analysis above (Figure 4). In both A1 and IC, the magnitude of firing rate modulation between passive blocks was significantly reduced after accounting for effects of pupil (A1: $p = 0.00120$, IC: $p = 9.39 \times 10^{-6}$, Wilcoxon signed-rank test). Accounting for arousal led to a 20% and a 48% reduction in P1 versus P2 modulation in A1 and IC, respectively (A1: mean signed-normalized MI_{P1P2} *block-only* = 0.140, MI_{P1P2} *block-unique* = 0.100; IC: mean signed-normalized MI_{P1P2} *block-only* = 0.100,

455 MI_{P1P2} *block-unique* = 0.052). While there was decrease in post-behavior effects on average,
456 there were distinct groups of units in both A1 and IC that showed changes between P1 and P2,
457 even after accounting for pupil (compare units falling on the unity line versus x-axis in Figure 7).
458 Thus, while some post-behavior effects previously reported as persistent plasticity induced by
459 behavior can in fact be explained by fluctuations in pupil-indexed arousal, a small number of
460 units showed persistent post-behavior changes, even after accounting for pupil.

461 **Discussion**

462 The goal of this study was to explore how arousal contributed to task-related changes in
463 neural activity in the primary auditory cortex (A1) and the auditory midbrain (IC). Several
464 previous studies have shown that transitioning from passive listening to active behavior leads to
465 sizable changes in neural activity in A1 (Fritz et al., 2003; Niwa et al., 2012; Otazu et al., 2009)
466 and IC (Ryan and Miller, 1977; Slee and David, 2015). These changes can be specific to
467 properties of the task stimuli (Fritz et al., 2003; Jaramillo and Zador, 2011; Lee and
468 Middlebrooks, 2011) or depend on the structural elements of the task, such as reward
469 contingencies (David et al., 2012), task difficulty (Atiani et al., 2009) or selective attention
470 (Hocherman et al., 1976; Lakatos et al., 2013; Schwartz and David, 2018). While it is clear that
471 sensory and behavioral context shapes auditory representation, a coherent theory of how multiple
472 state variables interact to influence sensory coding has yet to be formed.

473 Changes in firing rate associated with behavioral context are likely to reflect multiple
474 aspects of internal state (McGinley et al., 2015; Niell and Stryker, 2010; Polack et al., 2013).
475 Factors like arousal, locomotion, and whisking rate have been shown to change gradually over
476 the course of an experiment, tracking fluctuations in the membrane potential of sensory neurons
477 and behavioral performance (McGinley et al., 2015; Niell and Stryker, 2010; Poulet and
478 Petersen, 2008). A major obstacle to understanding the relationship between state variables and
479 firing rate is that state variables often covary (Musall et al., 2019; Stringer et al., 2019). To
480 overcome this obstacle and dissociate the effects of arousal and task engagement on cortical and
481 midbrain activity, we used a step-wise linear regression approach in which pupil-indexed arousal
482 and task engagement provided separate regressors. In about half of A1 and IC units, arousal
483 and/or task engagement modulated spiking activity between blocks of active engagement and

passive listening. The behavioral state variable changes are correlated; that is, arousal tends to increase during task engagement. However, they affect independent neural populations, suggesting that effects of arousal and other aspects of task engagement operate via distinct feedback circuits.

Reinterpreting previous studies of auditory behavior

Our findings indicate that changes in firing rate previously attributed to task engagement might instead reflect fluctuations in pupil-indexed arousal, particularly in IC, where pupil-related changes predominate. Changes in arousal can also explain some modulation that persists after behavior ceases (Fritz et al., 2003; Slee and David, 2015). However, arousal did not account for all the modulation between active and passive blocks; instead it appears that both arousal and task engagement act on independent neural populations to shape sound processing. Previous studies that measured the effects of task engagement on auditory neuronal activity described different effects on overall excitability between A1 and IC. In A1 the effects of task engagement were shown to be enhancing (David et al., 2012), while in IC these changes were predominantly suppressive (Slee and David, 2015). Separate studies have shown that pupil size is positively correlated with excitability in both A1 and IC (Joshi et al., 2016; Schwartz et al., 2020). We also found that increased arousal enhanced excitability in both areas. However, after accounting for pupil-related changes, task-engagement effects were no longer enhancing in A1, and they were more suppressive in IC. Pupil-related changes did not depend on tuning for the target tone. These non-specific effects of arousal contrasted with effects of task engagement, which can be selective for task-relevant features (Fritz et al., 2003; Kuchibhotla et al., 2017; Slee and David, 2015).

In the current study, significant state-dependent A1 units were equally likely to be modulated by task, by arousal, or by both. In IC, however, we found that a larger portion of state-dependent changes could be explained by arousal. Furthermore, in IC but not in A1, units with less reliable auditory responsiveness were those with a stronger state-modulation component. This result is perhaps not surprising given that the majority of IC units in our sample were recorded from regions of the IC marked as non-central (NCIC). These are dorsal and lateral regions of IC that receive input from brain neuromodulatory nuclei such as the pedunculopontine and latero-dorsal tegmental nuclei (Motts and Schofield, 2009), as well as multisensory information from somatosensory, visual, and oculomotor centers (Gruters and Groh, 2012). These results suggest that the auditory midbrain is not a passive sound processor. Instead, the network of midbrain nuclei in the IC plays an active role enhancing behaviorally relevant signals. Further experiments, which include a larger sample of units across the different areas would be needed to confirm the interplay of behavioral and sensory signals in IC.

Multiple regression has been used previously to dissociate effects of arousal and movement on neural activity (Musall et al., 2019; Stringer et al., 2019). This study used this approach to dissociate the effects of state-related variables and differentiate where effects emerge. Several other variables have been show to impact auditory responses during behavior, including selective attention, temporal expectation, reward value and motor responses (David et al., 2012; Huang et al., 2019; Jaramillo and Zador, 2011; Lakatos et al., 2013; Metzger et al., 2006). The same method can be adopted to explore the contribution of other state variables measured in normal conditions as well as in perturbation experiments to identify the circuits through which such variables operate.

Defining meaningful state variables

The correlation between pupil-indexed arousal and task engagement demonstrates the importance of accounting for correlations between state variables when measuring their effects on neural activity. Related to this problem is the question of what constitutes a meaningful measure of behavioral state. Classic concepts from psychology, such as "selective attention" make intuitive sense in that they can be observed rigorously in behavior (Posner et al., 1980). However, there remains no clear physiological correlate for attention. Recent work has argued instead that attentional effects arise from separable signals, such as those associated with motivation and reward (Baruni et al., 2015; Luo and Maunsell, 2015). Moreover, attention reflects population activity across a neural network, rather than a single identifiable control signal (Cohen and Maunsell, 2009) and its effects differ across sensory modalities (Woodruff et al., 1996). Thus, while attention may be observed as a relatively simple behavioral variable, it emerges from a constellation of neurophysiological processes.

Arousal and task engagement may be regarded as similarly slippery concepts that cannot be pinned to distinct physiological processes. The nonspecific mechanisms underlying these behaviorally-defined variables contrasts with pupil diameter, which has a clear link to neurophysiology (McGinley et al., 2015; Reimer et al., 2016; Zekveld et al., 2018). The detailed circuits that link pupil diameter to cognitive state are not fully understood, but the connection to behavioral state has been demonstrated repeatedly. Pupil size may not map onto a single, simple cognitive variable, but it has a clear link to brain mechanisms. Similarly, motor- and reward-related activity can be readily linked to specific neural circuits (Bakin and Weinberger, 1990; Schneider et al., 2014). State variables that can be linked to specific neural circuits or systems

may provide clearer insight into the link between behavior and sensory processing, in contrast to concepts founded exclusively on studies of psychology and behavior.

Possible circuits mediating task and arousal-related modulation in A1 and IC

Probing the neural circuits underling task and arousal-related modulation was outside the scope of this study. However, by measuring the relationship between the unique contributions of each state variable, we were able to conclude that the effects of task and arousal are dissociated and may be carried via different pathways.

Several previous studies have shown the role of neuromodulators in inducing short-term changes in activity and sensory tuning in cortex (Bakin and Weinberger, 1996; Goard and Dan, 2009) and midbrain (Gittelman et al., 2013; Habbicht and Vater, 1996; Hurley and Pollak, 2005). Cholinergic fibers projecting to the auditory cortex from the nucleus basalis play a key role in rapid switching between passive listening and active engagement by modulating the activity of different populations of cortical inhibitory interneurons (Kuchibhotla et al., 2017). Furthermore, the activity of cholinergic and noradrenergic terminals in auditory cortex was found to be elevated during pupil dilation and reduced during pupil constriction (Reimer et al., 2016). Given that we find that modulation of task and pupil often covary, it is reasonable to hypothesize that cholinergic and noradrenergic pathways support these aspects of cognition.

569 **Materials and Methods**

570 All procedures were approved by the Oregon Health and Science University Institutional
571 Animal Care and Use Committee and conform to the National Institutes of Health standards.
572

573 **Surgical procedure**

574 Animal care and procedures were similar to those described previously for
575 neurophysiological recordings from awake behaving ferrets (Slee and David, 2015). Four young
576 adult male ferrets were obtained from an animal supplier (Marshall Farms, North Rose, NY).
577 After a two-week quarantine, a sterile surgery was performed under isoflurane anesthesia to
578 mount two head-posts for head fixation and to permit access to auditory brain regions for
579 recordings. A UV light-cured composite (Charisma, Heraeus Kulzer International) mount two
580 custom-made stainless-steel head-posts spaced approximately 1 cm apart along the sagittal crest
581 of the skull. The stability of the implant was achieved using 8-10 stainless steel bone screws
582 mounted in the skull (Depuy Synthes, Raynham, MA), which were covered along with the
583 headpost in additional Charisma and acrylic denture material (Co-oral-ite Dental, Diamond
584 Springs. CA). Two 1.2x1.2 cm wells over auditory cortex in the implant were covered with only
585 a thin layer of Charisma to allow access to auditory regions.

586 Following surgery, animals were treated with prophylactic antibiotics (Baytril 10 mg/kg)
587 and analgesics (Buprenorphin 0.02 mg/kg) under the supervision of University veterinary staff.
588 For the first two weeks the wound was cleaned with antiseptics (Betadine 1:4 in saline and
589 Chlorhexidine 0.2%) and bandaged daily with application of topic antibiotic ointment
590 (Bacitracin). After the wound margin was healed, cleaning and bandaging occurred every 2-3
591 days through the life of the animals. This method revealed to be very effective in minimizing

infections of the wound margin. After recovery (~2 weeks), animals were habituated to a head-fixed posture inside the sound-booth chamber for about 2 weeks prior to the beginning of the training.

Behavioral paradigm and training

The animals were trained by instrumental conditioning to perform a positively reinforced, tone versus noise discrimination task (Ferret L) (Slee and David, 2015) or tone-in-noise detection task (Ferrets R, B, T) . During training, animals were provided access to water *ad libitum* on weekends, but were placed on water restriction during the weekdays (Monday through Friday), allowing them to maintain >90% of their baseline body weight long-term. On weekdays, they were given the opportunity to receive liquid reward during behavioral training. Each behavioral trial consisted of a sequence of 2-5 broadband noise reference sounds (TORCs; 30 samples, 5 octaves, 0.75 s duration, 0.7 s inter-stimulus interval)(Klein et al., 2000), followed by a target tone, either alone (tone versus noise task) or overlapping with another TORC (tone-in-noise task). Animals reported the occurrence of the target by licking a water spout (Figure 1A). Licks were detected by a piezoelectric sensor glued to the spout. Licks occurring within the target window, 0.1-1.4 s after target onset, were rewarded with 1-3 drops of a 2:1 solution of water and Ensure. False alarms, licks occurring before the target window, and misses, a failure to lick during the target window, resulted in a 5-8 seconds timeout. Animals were then required to no lick for a random period (2.5 ± 0.5 s) before the next trial began. The number of TORCs per trial was distributed randomly with a flat hazard function to prevent behavioral timing strategies (Heffner and Heffner, 1995). Behavioral performance was measured using *d'*, the z-scored difference between hit rate and false alarm rate (Green and Swets, 1966)

A behavioral block consisted of 60-100 trials with the same target tone frequency (100 – 20,000 Hz) and same distribution of target signal-to-noise ratio (SNR). Animals completed 1-3 behavioral blocks per day, between which target frequency and/or SNR could change. During training, target frequency was chosen at random to span the audiogram of a ferret (Kelly et al., 1986). During electrophysiological recordings, target tone frequency was selected to match the best frequency of the recording site.

During the training on the tone-in-noise variant of the task, the TORC sample masking the target varied randomly in each trial to prevent animals from using TORCs' spectro-temporal features to identify targets. At the beginning of training, the tone was presented at +40 dB signal-to-noise ratio (SNR; ratio of peak-to-peak amplitude) relative to the TORCs. This difference was gradually reduced over the course of two-three weeks until the animal consistently performed above chance (three behavioral blocks with performance yielding to > 0.5 discrimination index, see below) at 0dB SNR.

For the tone-in-noise task, the SNR of the tone with respect to the overall level of the TORCs (fixed at 55 or 60dB SPL depending on the animal) varied between +5 and -20dB SNR, in 5dB steps. Each session included five target/noise SNRs. To manipulate task difficulty within each session, the probability of each of the five target/noise SNRs varied, yielding two difficulty conditions: a high SNR ("easy") condition in which 60% of the trials the target/noise SNR was either the highest or the second to the highest SNR within the target/noise SNR distribution; and a low SNR ("hard") condition in which the two lowest target/noise SNRs occurred in 60% of the trials. For example, for ferret B, the distribution after training was completed was kept between 0 and -20dB SNR, so that in the easy condition 0 and -5dB SNR targets would appear 60% of the time, -10dB SNR 20% of the time, and the remaining -15 and -20dB SNR would be presented

638 another 20% of the trials. During electrophysiological tone-in-noise experiments, the tone was
639 embedded in a single TORC sample, which also occurred in the reference period. We confirmed
640 that animals were not biased to respond to this TORC exemplar in the reference phase.
641
642 **Sound presentation**
643 Behavioral training and subsequent neurophysiological recording took place in a sound-
644 attenuating chamber (Gretch-Ken) with a custom double-wall insert. Stimulus presentation and
645 behavior were controlled by custom MATLAB software (code available at
646 https://bitbucket.org/lbhb/baphy). Digital acoustic signals were transformed to analog (National
647 Instruments), amplified (Crown), and delivered through two free-field speakers (Manger, 50-35
648 000 Hz flat gain) positioned ±30 degrees azimuth and 80 cm distant from the animal. Stimuli
649 were presented either from the left or the right speaker, contralaterally to the recording site.
650 Sound level was equalized and calibrated against a standard reference (Brüel & Kjær).
651
652 **Pupil recording**
653 During experiments, infrared video of one eye was collected for offline measurement of
654 pupil size as an index of arousal. Ambient light was maintained at a constant level to prevent
655 light-evoked changes in pupil and to maximize the dynamic range of arousal-related changes
656 (Schwartz et al., 2020). Recordings were collected using a CCD camera (Adafruit TTL Serial
657 Camera 397) fitted with a lens (M12 Lenses PT-2514BMP 25.0 mm) whose focal length allowed
658 placement of the camera 10 cm from the eye. To improve contrast, the imaged eye was
659 illuminated by a bank of infrared LEDs. Ambient luminance was provided using a ring light
660 (AmScope LED-144S). At the start of each recording day, the intensity of the ring light was set

661 to a level (~1500 lux measured at the recorded eye) chosen to give a maximum dynamic range of
662 pupil sizes. Light intensity remained fixed across the recording session. Pupil diameter was
663 measured from the video signal offline using custom MATLAB software, which is detailed in
664 (Schwartz et al., 2020).
665
666 **Neurophysiology**
667 After animals demonstrated consistent above-chance performance (target versus
668 reference *d*' > 1, see below), a small craniotomy was opened to access either primary auditory
669 cortex (A1) (Schwartz and David, 2018) or inferior colliculus (IC) (Slee and David, 2015).
670 Extracellular neuronal activity was recorded in non-anesthetized ferrets either using a tetrode
671 (Thomas Recording Inc.), or a linear 64-channel silicon probe (Shobe et al., 2015). The
672 impedance of the tetrode was measured to be 1-2 MOhm, and the 64-channel probe was
673 electroplated to reach a 0.7-MOhm impedance in each channel. The tetrode and probe were
674 inserted using a motorized electrode positioning system (Alpha-Omega).
675 Amplified (tetrodes, AM Systems; arrays, Intan) and digitized (National Instruments)
676 electrophysiological signals were stored using the open-source data acquisition software
677 MANTA (Englitz et al., 2013) or Open Ephys (Black et al., 2017). Recording sites in A1 were
678 confirmed based on tonotopy and relatively reliable and simple response properties (Shamma et
679 al., 1993). Recording sites in the IC were determined by tonotopy and response properties
680 (Aitkin et al., 1975; Moore et al., 1983). Neurons in the central nucleus of the IC (here referred
681 to as ICC) receive input from the auditory brainstem, and have a characteristic short response
682 latency, dorsal-ventral tonotopy, and narrow bandwidth tuning. Conversely, regions around the
683 central nucleus do not receive direct ascending input and present longer response latencies,

684 considerably less sharp tuning, lack consistent tonotopic organization; these areas were grouped
685 together as NCIC (Slee and David, 2015).
686 For tetrode recordings, upon unit isolation, a series of brief (100-ms duration, 200-400ms
687 inter-stimulus interval, 50 dB SPL) tones and/or narrowband noise bursts were used to determine
688 the range of frequencies that evoked the strongest response, the best frequency (BF) of the
689 unit(s). If a unit(s) in the site did not respond to the sound stimuli (an evoked increase or
690 decrease in activity compared to spontaneous activity either during or after sound presentation),
691 the electrode was moved to a new recording depth with small, 5um incremental steps. For the 64-
692 channel recordings, we lowered the probe so that its entire extent (1 mm) spanned the target
693 region (A1 or IC).
694
695 *Spike sorting*
696 Putative spikes were sorted offline by band-pass filtering the raw trace (300–6000 Hz)
697 and extracting events from the continuous signal that deviated ≥4 standard deviations from zero.
698 To separate single units and stable multi units from the electrode signal, we used the Catamaran
699 clustering program (kindly provided by D. Schwarz and L. Carney) (Schwarz et al., 2012) for
700 tetrode recordings, and the software KiloSort (Pachitariu et al., 2016) for array recordings. In
701 both cases, units were defined based on visual inspection of traces and by having less than 1% of
702 inter-spike intervals shorter than 0.75 ms (single units) and less than 2.5% inter-spike intervals
703 shorter than 0.75ms (multi units). Stability of single-unit isolation was verified by examining
704 waveforms and interval histograms. If isolation was lost during an experiment, only activity
705 during the stable period was analyzed.
706

707 **Analysis**

708 *Task performance*

709 Behavioral performance was measured using signal detection theory (Green and Swets,
710 1966; Stanislaw and Todorov, 1999). Hits or false alarms (*FAs*) occurred when the animal licked
711 the piezo waterspout upon presentation of the target or the reference stimuli, respectively. Misses
712 or correct rejections (*CRs*) occurred when the animal did not lick following presentation of the
713 target or reference. Hit rate (*HR*) was calculated as the proportion of licks that occurred upon
714 presentation of the target during the response window (0.1 to 1.5 s after target onset), $HR = hits /$
715 $(hits+misses)$. False alarm rate (*FAR*) was calculated as the proportion of reference stimuli that
716 elicited a lick, during the same window following reference onset, $FAR = FAs / (FAs + CRs)$.
717 Sensitivity (d'), a measure of the animals' ability to discriminate between target tone and
718 reference noise, was measured by the difference between the z-scored hit rate and the false alarm
719 rate, $d' = HR_z - FAR_z$. No discrimination, that is, equal likelihood of responding to target and
720 reference is indicated by $d' = 0$. Animals were considered trained to the task and ready to
721 undergo electrophysiological recordings when they performed consistently above chance ($d' > 1$)
722 for three consecutive sessions.

723

724 *Auditory tuning properties*

725 Tuning properties of A1 and IC neurons were characterized using the spectro-temporal
726 receptive field (STRF) estimated by reverse correlation between time-varying neuronal spike rate
727 and the rippled noise used as reference sounds during behavior (Klein et al., 2000). The STRF
728 provides a quick and efficient measure of stimulus frequencies that enhance or suppress neural
729 firing. In the current study, the STRF was used to measure best frequency (BF) as the center of

mass of a spectral tuning curve computed from the first principle component of the STRF matrix (Simon et al., 2007). Auditory responsiveness was computed as the signal-to-noise ratio of single trial responses to the reference noise stimuli during passive listening (Klein et al., 2000).

State-dependent models

We fit a generalized linear model in which time-varying state variables, pupil-indexed arousal, $p(t)$, and task engagement, $b(t)$, were used to re-weight each neuron's mean evoked response to each noise stimulus, $r_0(t)$, and spontaneous rate, s_0, to generate a prediction of the single-trial spike rate, $r_{full}(t)$, at each point in time. The model included multiplicative gain parameters (g) and DC offset parameters (d) to capture both types of modulation. We refer to this model as the *full model*:

$$r_{full}(t) = s_0 F_d\left[d_0 + d_p p(t) + d_b b(t)\right] + r_0(t) F_g\left[g_0 + g_p p(t) + g_b b(t)\right] \quad (1).$$

To account for nonlinear threshold and saturation of state effects, the summed state signal was passed through a sigmoid nonlinearity, F_d or F_g, before scaling response baseline or gain, respectively (difference of exponentials) (Thorson et al., 2015). With additional constant terms g_0 and d_0, this model required a total of six free parameters. For comparison, we calculated a state-independent model here referred to as the *null model*, in which the state variable regressors were shuffled in time. Because shuffling removes any possible correlation between state and neural activity, gain and offset parameters are reduced to d_0=g_0=1 and d_p=d_b=g_p=g_b=0, effectively reducing the model to

$$r_{null}(t) = s_0 + r_0(t) \quad (2).$$

In practice, fitting to the shuffled data produces parameter values slightly different from zero, and controls for noise in the regression procedure.

We also considered two *partial models*, one to predict responses based on pupil size only, $r_p(t)$, and one to predict responses based on behavior only, $r_b(t)$, in which the other regressor was shuffled in time. Thus, the pupil-only model accounted only for effects of pupil-indexed arousal,

$$r_p(t) = s_0 F_d\left[d_0 + d_p p(t)\right] + r_0(t) F_g\left[g_0 + g_p p(t)\right] \quad (3),$$

and the task-only model accounted only for task engagement,

$$r_b(t) = s_0 F_d\left[d_0 + d_b b(t)\right] + r_0(t) F_g\left[g_0 + g_b b(t)\right] \quad (4).$$

These models tested the effects of a single state variable while ignoring the other.

By comparing performance of the full model to each partial model, we determined the unique contribution of each state variable to the neuron's activity. We used a 20-fold cross validation procedure to evaluate model performance. The model was fit to 95% of the data and used to predict the remaining 5%. Fit and test data were taken from interleaved trials. This procedure was repeated 20 times with non-overlapping test sets, so that the final result was a prediction of the entire response. Model performance was then quantified by the fraction of variance explained, *i.e.*, the squared correlation coefficient, r^2, between the predicted and actual time-varying response. Variance uniquely explained by single state variables was calculated as the difference between r^2 for the full model and for the partial model in which the relevant variable was shuffled in time.

When comparing pupil and neural data, a 750-ms offset was applied to pupil trace to account for the lagged relationship between changes in pupil size and neural activity in auditory cortex (McGinley et al., 2015).

Modulation Index

To quantify the modulatory effects of task and arousal on the firing rate of A1 and IC units, we computed a modulation index (*MI*) (Otazu et al., 2009; Schwartz and David, 2018). *MI* was defined as the difference between the mean response to the same stimuli in two conditions, α and β, normalized by the sum,

$$MI_{\alpha\beta} = \frac{r_\alpha - r_\beta}{r_\alpha + r_\beta} \quad (5).$$

MI could be calculated between different behavioral blocks or between state conditions. In the case of task engagement, *MI* was calculated between active and passive conditions, MI_{AP}. For arousal, data from an experiment were divided at the median pupil diameter, and *MI* was computed between large pupil (above median, high arousal) and small pupil (below median, low arousal), MI_{LS}. To quantify differences between the first and the second passives, *MI* was computed between the first and second passive blocks, MI_{P1P2}.

To quantify changes in firing rates due to unique contributions of arousal or task, we used *MI* to test how well the regression model could predict state-related changes in neural activity. The modulation between conditions α and β predicted by the full model, is denoted $MI_{\alpha\beta}$ *full*, where α and β are either active/passive (MI_{AP} *full*) or large/small pupil (MI_{LS} *full*). Similarly, modulations between conditions α and β predicted by the pupil partial model or the behavior partial model, are denoted $MI_{\alpha\beta}$ *pupil-only* and $MI_{\alpha\beta}$ *task-only*, respectively. The *MI* uniquely predicted by including task engagement as a regressor is

$$MI_{AP}\ task\ unique = MI_{AP}\ full - MI_{AP}\ pupil\ only \quad (6),$$

that is, *MI* predicted by the full model minus *MI* predicted by a model in which behavior condition, but not pupil, is shuffled. The net result is the *MI* predicted by task engagement above

and beyond modulation predicted by changes in arousal alone. Similarly, *MI* uniquely predicted by including pupil size as a regressor is

$$MI_{LS}\ pupil\ unique = MI_{LS}\ full - MI_{LS}\ task\ only \quad (7).$$

Significant effects of regressing out pupil-indexed arousal were quantified by comparing the signed-normalized differences between MI_{AP} *task-unique* and MI_{AP} *task-only* using a one-sided Wilcoxon signed-rank test with an $\alpha = 0.05$, including zero-differences between the two (Pratt treatment). Differences of the same quantities across areas were quantified using rank-sum test. Sign normalization was achieved by multiplying the difference between MI_{AP} *task-unique* and MI_{AP} *task-only* in each unit by the sign of their mean.

Significantly modulated units were determined by comparing Pearson's *r* coefficients associated with the full model and with the difference between the full model and the task and pupil partial models using jackknifed *t*-test with $\alpha = 0.05$ (Efron and Tibshirani, 1986).

Data preprocessing and analysis were performed using custom MATLAB and Python scripts. Neural and pupil activity were binned at 20 samples/s before analysis. A Python library for the modeling portion of this analysis is available at https://github.com/LBHB/NEMS/.

References Cited

Aitkin LM, Webster WR, Veale JL, Crosby DC. 1975. Inferior colliculus. I. Comparison of response properties of neurons in central, pericentral, and external nuclei of adult cat. *J Neurophysiol* **38**:1196–1207.

Atiani S, David SV, Elgueda D, Locastro M, Radtke-Schuller S, Shamma SA, Fritz JB. 2014. Emergent selectivity for task-relevant stimuli in higher-order auditory cortex. *Neuron* **82**:486–499. doi:10.1016/j.neuron.2014.02.029

Atiani S, Elhilali M, David SV, Fritz JB, Shamma SA. 2009. Task difficulty and performance induce diverse adaptive patterns in gain and shape of primary auditory cortical receptive fields. *Neuron* **61**:467–480.

Bagur S, Averseng M, Elgueda D, David S, Fritz J, Yin P, Shamma S, Boubenec Y, Ostojic S. 2018. Go/No-Go task engagement enhances population representation of target stimuli in primary auditory cortex. *Nat Commun* **9**:2529. doi:10.1038/s41467-018-04839-9

Bakin JS, Weinberger NM. 1996. Induction of a physiological memory in the cerebral cortex by stimulation of the nucleus basalis. *Proc Natl Acad Sci U A* **93**:11219–11224.

Bakin JS, Weinberger NM. 1990. Classical conditioning induces CS-specific receptive field plasticity in the auditory cortex of the guinea pig. *Brain Res* **536**:271–86.

Baruni JK, Lau B, Salzman CD. 2015. Reward expectation differentially modulates attentional behavior and activity in visual area V4. *Nat Neurosci* **18**:1656–63. doi:10.1038/nn.4141

Beaton R, Miller JM. 1975. Single cell activity in the auditory cortex of the unanesthetized, behaving monkey: Correlation with stimulus controlled behavior. *Brain Res* **100**:543–62. doi:10.1016/0006-8993(75)90157-2

Beatty J. 1982. Task-evoked pupillary responses, processing load, and the structure of processing resources. *Psychol Bull* **91**:276–92.

Bizley JK, Cohen YE. 2013. The what, where and how of auditory-object perception. *Nat Rev Neurosci* **14**:693–707. doi:10.1038/nrn3565

Bizley JK, Walker KMM, Nodal FR, King AJ, Schnupp JWH. 2013. Auditory cortex represents both pitch judgments and the corresponding acoustic cues. *Curr Biol* **23**:620–5. doi:10.1016/j.cub.2013.03.003

Black C, Voigts J, Agrawal U, Ladow M, Santoyo J, Moore C, Jones S. 2017. Open Ephys electroencephalography (Open Ephys + EEG): a modular, low-cost, open-source solution to human neural recording. *J Neural Eng* **14**:035002. doi:10.1088/1741-2552/aa651f

Brosch M, Selezneva E, Scheich H. 2005. Nonauditory events of a behavioral procedure activate auditory cortex of highly trained monkeys. *J Neurosci* **25**:6797–6806.

Cohen MR, Maunsell JHR. 2009. Attention improves performance primarily by reducing interneuronal correlations. *Nat Neurosci* **12**:1594–1600. doi:10.1038/nn.2439

David SV, Fritz JB, Shamma SA. 2012. Task reward structure shapes rapid receptive field plasticity in auditory cortex. *Proc Natl Acad Sci USA* **109**:2150–55. doi:10.1073/pnas.1117717109

Downer JD, Niwa M, Sutter ML. 2015. Task engagement selectively modulates neural correlations in primary auditory cortex. *J Neurosci* **35**:7565–7574. doi:10.1523/JNEUROSCI.4094-14.2015

Efron B, Tibshirani R. 1986. Bootstrap methods for standard errors, confidence intervals, and other measures of statistical accuracy. *Stat Sci* **1**:54–77.

Eliades SJ, Wang X. 2008. Neural substrates of vocalization feedback monitoring in primate auditory cortex. *Nature* **453**:1102–6. doi:10.1038/nature06910

Englitz B, David SV, Sorenson MD, Shamma SA. 2013. MANTA-an open-source, high density electrophysiology recording suite for MATLAB. *Front Neural Circuits* **7**:69. doi:10.3389/fncir.2013.00069

Fritz JB, David SV, Radtke-Schuller S, Yin P, Shamma SA, Elhilali M. 2010. Adaptive, behaviorally gated, persistent encoding of task-relevant auditory information in ferret frontal cortex. *Nat Neurosci* **13**:1011–9. doi:10.1038/nn.2598

Fritz JB, Elhilali M, David SV, Shamma SA. 2007. Does attention play a role in dynamic receptive field adaptation to changing acoustic salience in A1? *Hear Res* **229**:186–203.

Fritz JB, Elhilali M, Shamma SA. 2005. Differential dynamic plasticity of A1 receptive fields during multiple spectral tasks. *J Neurosci* **25**:7623–7635.

Fritz JB, Shamma SA, Elhilali M, Klein DJ. 2003. Rapid task-related plasticity of spectrotemporal receptive fields in primary auditory cortex. *Nat Neurosci* **6**:1216–1223.

Fu Y, Tucciarone JM, Espinosa JS, Sheng N, Darcy DP, Nicoll RA, Huang ZJ, Stryker MP. 2014. A cortical circuit for gain control by behavioral state. *Cell* **156**:1139–1152. doi:10.1016/j.cell.2014.01.050

Gilzenrat MS, Nieuwenhuis S, Jepma M, Cohen JD. 2010. Pupil diameter tracks changes in control state predicted by the adaptive gain theory of locus coeruleus function. *Cogn Affect Behav Neurosci* **10**:252–69. doi:10.3758/CABN.10.2.252

Gittelman JX, Perkel DJ, Portfors CV. 2013. Dopamine modulates auditory responses in the inferior colliculus in a heterogeneous manner. *J Assoc Res Otolaryngol* **14**:719–729.

871 Goard M, Dan Y. 2009. Basal forebrain activation enhances cortical coding of natural scenes.
872 *Nat Neurosci* **12**:1444–1449.
873 Green DM, Swets J. 1966. Signal detection theory and psychophysics. New York: Wiley.
874 Gruters KG, Groh JM. 2012. Sounds and beyond: multisensory and other non-auditory signals in
875 the inferior colliculus. *Front Neural Circuits* **6**:96. doi:10.3389/fncir.2012.00096
876 Habbicht H, Vater M. 1996. A microiontophoretic study of acetylcholine effects in the inferior
877 colliculus of horseshoe bats: implications for a modulatory role. *Brain Res* **724**:169–179.
878 Heffner HE, Heffner RS. 1995. Conditioned Avoidance In: Klump GM, Dooling RJ, Fay RR,
879 Stebbins WC, editors. Methods in Comparative Psychoacoustics. Basel: Birkhauser
880 Verlag. pp. 79–93.
881 Hocherman S, Benson DA, Goldstein Jr. MH, Heffner HE, Hienz RD. 1976. Evoked unit activity
882 in auditory cortex of monkeys performing a selective attention task. *Brain Res* **117**:51–
883 68.
884 Huang Y, Heil P, Brosch M. 2019. Associations between sounds and actions in early auditory
885 cortex of nonhuman primates. *Elife* **8**:e43281.
886 Hurley LM, Pollak GD. 2005. Serotonin shifts first-spike latencies of inferior colliculus neurons.
887 *J Neurosci* **25**:7876–7886.
888 Jaramillo S, Zador AM. 2011. The auditory cortex mediates the perceptual effects of acoustic
889 temporal expectation. *Nat Neurosci* **14**:246–51. doi:10.1038/nn.2688
890 Joshi S, Li Y, Kalwani RM, Gold JI. 2016. Relationships between Pupil Diameter and Neuronal
891 Activity in the Locus Coeruleus, Colliculi, and Cingulate Cortex. *Neuron* **89**:221–34.
892 doi:10.1016/j.neuron.2015.11.028
893 Kahneman D, Beatty J. 1966. Pupil diameter and load on memory. *Science* **154**:1583–5.

894 Kelly JB, Kavanagh GL, Dalton JC. 1986. Hearing in the ferret (Mustela putorius): thresholds
895 for pure tone detection. *Hear Res* **24**:269–75.
896 Klein DJ, Depireux DA, Simon JZ, Shamma SA. 2000. Robust spectrotemporal reverse
897 correlation for the auditory system: Optimizing stimulus design. *J Comput Neurosci*
898 **9**:85–111.
899 Knudsen DP, Gentner TQ. 2013. Active recognition enhances the representation of behaviorally
900 relevant information in single auditory forebrain neurons. *J Neurophysiol* **109**:1690–
901 1703. doi:10.1152/jn.00461.2012
902 Kuchibhotla KV, Gill JV, Lindsay GW, Papadoyannis ES, Field RE, Sten TAHH, Miller KD,
903 Froemke RC. 2017. Parallel processing by cortical inhibition enables context-dependent
904 behavior. *Nat Neurosci* **20**:62–71. doi:10.1038/nn.4436
905 Lakatos P, Musacchia G, O'Connel MN, Falchier AY, Javitt DC, Schroeder CE. 2013. The
906 spectrotemporal filter mechanism of auditory selective attention. *Neuron* **77**:750–61.
907 doi:10.1016/j.neuron.2012.11.034
908 Lee C-CC, Middlebrooks JC. 2011. Auditory cortex spatial sensitivity sharpens during task
909 performance. *Nat Neurosci* **14**:108–14. doi:10.1038/nn.2713
910 Lin P-A, Asinof SK, Edwards NJ, Isaacson JS. 2019. Arousal regulates frequency tuning in
911 primary auditory cortex. *Proc Natl Acad Sci* **116**:25304–25310.
912 doi:10.1073/pnas.1911383116
913 Luo TZ, Maunsell JHR. 2015. Neuronal Modulations in Visual Cortex Are Associated with Only
914 One of Multiple Components of Attention. *Neuron* **86**:1182–1188.
915 doi:10.1016/j.neuron.2015.05.007

McGinley MJ, David SV, McCormick DA. 2015. Cortical membrane potential signature of optimal states for sensory signal detection. *Neuron* **87**:179–192.

Metzger RR, Greene NT, Porter KK, Groh JM. 2006. Effects of reward and behavioral context on neural activity in the primate inferior colliculus. *J Neurosci* **26**:7468–7476.

Moore DR, Semple MN, Addison PD. 1983. Some acoustic properties of neurones in the ferret inferior colliculus. *Brain Res* **269**:69–82.

Motts SD, Schofield BR. 2009. Sources of cholinergic input to the inferior colliculus. *Neuroscience* **160**:103–14. doi:10.1016/j.neuroscience.2009.02.036

Musall S, Kaufman MT, Juavinett AL, Gluf S, Churchland AK. 2019. Single-trial neural dynamics are dominated by richly varied movements. *Nat Neurosci* **22**:1677–1686. doi:10.1038/s41593-019-0502-4

Niell CM, Stryker MP. 2010. Modulation of Visual Responses by Behavioral State in Mouse Visual Cortex. *Neuron* **65**:472–479. doi:10.1016/j.neuron.2010.01.033

Niwa M, Johnson JS, O'Connor KN, Sutter ML. 2012. Active engagement improves primary auditory cortical neurons' ability to discriminate temporal modulation. *J Neurosci* **32**:9323–34. doi:10.1523/JNEUROSCI.5832-11.2012

Otazu GH, Tai L-HH, Yang Y, Zador AM. 2009. Engaging in an auditory task suppresses responses in auditory cortex. *Nat Neurosci* **12**:646–54. doi:10.1038/nn.2306

Pachitariu M, Steinmetz N, Kadir S, Carandini M, Harris KD. 2016. Kilosort: realtime spike-sorting for extracellular electrophysiology with hundreds of channels. doi:10.1101/061481

Polack PO, Friedman J, Golshani P. 2013. Cellular mechanisms of brain state-dependent gain modulation in visual cortex. *Nat Neurosci* **16**:1331–1339. doi:10.1038/nn.3464

Posner MI, Snyder CRR, Davidson BJ. 1980. Attention and the detection of signals Journal of Experimental Psychology.

Poulet JFA, Petersen CCH. 2008. Internal brain state regulates membrane potential synchrony in barrel cortex of behaving mice. *Nature* **454**:881–5. doi:10.1038/nature07150

Reimer J, McGinley MJ, Liu Y, Rodenkirch C, Wang Q, McCormick DA, Tolias AS. 2016. Pupil fluctuations track rapid changes in adrenergic and cholinergic activity in cortex. *Nat Commun* **7**:13289. doi:10.1038/ncomms13289

Ringach DL. 2009. Spontaneous and driven cortical activity: implications for computation. *Curr Opin Neurobiol* **19**:439–444. doi:10.1016/j.conb.2009.07.005

Ryan AF, Miller JM. 1977. Effects of behavioral performance on single-unit firing patterns in inferior colliculus of the rhesus monkey. *J Neurophysiol* **40**:943–56.

Schneider DM, Nelson A, Mooney R. 2014. A synaptic and circuit basis for corollary discharge in the auditory cortex. *Nature* **513**:189–94. doi:10.1038/nature13724

Schriver BJ, Bagdasarov S, Wang Q. 2018. Pupil-linked arousal modulates behavior in rats performing a whisker deflection direction discrimination task. *J Neurophysiol* **120**:1655–1670. doi:10.1152/jn.00290.2018

Schwartz ZP, Buran BN, David SV. 2020. Pupil-associated states modulate excitability but not stimulus selectivity in primary auditory cortex. *J Neurophysiol* **123**:191–208. doi:10.1152/jn.00595.2019

Schwartz ZP, David SV. 2018. Focal suppression of distractor sounds by selective attention in auditory cortex. *Cereb Cortex N Y N 1991* **28**:323–339. doi:10.1093/cercor/bhx288

Schwarz DM, Zilany MSA, Skevington M, Huang NJ, Flynn BC, Carney LH. 2012. Semi-supervised spike sorting using pattern matching and a scaled Mahalanobis distance metric. *J Neurosci Methods* **206**:120–31. doi:10.1016/j.jneumeth.2012.02.013

Shamma SA, Fleshman JW, Wiser PR, Versnel H. 1993. Organization of response areas in ferret primary auditory cortex. *J Neurophysiol* **69**:367–83.

Shobe JL, Claar LD, Parhami S, Bakhurin KI, Masmanidis SC. 2015. Brain activity mapping at multiple scales with silicon microprobes containing 1,024 electrodes. *J Neurophysiol* **114**:2043–52. doi:10.1152/jn.00464.2015

Simon JZ, Depireux DA, Klein DJ, Fritz JB, Shamma SA. 2007. Temporal symmetry in primary auditory cortex: implications for cortical connectivity. *Neural Comput* **19**:583–638. doi:10.1162/neco.2007.19.3.583

Slee SJ, David SV. 2015. Rapid task-related plasticity of spectro-temporal receptive fields in the auditory midbrain. *J Neurosci* **35**:13090–102. doi:10.1523/JNEUROSCI.1671-15.2015

Stanislaw H, Todorov N. 1999. Calculation of signal detection theory measures. *Behav Res Methods Instrum Comput J Psychon Soc Inc* **31**:137–49.

Stringer C, Pachitariu M, Steinmetz N, Reddy CB, Carandini M, Harris KD. 2019. Spontaneous behaviors drive multidimensional, brainwide activity. *Science* **364**. doi:10.1126/science.aav7893

Tsunada J, Liu ASK, Gold JI, Cohen YE. 2015. Causal contribution of primate auditory cortex to auditory perceptual decision-making. *Nat Neurosci* **19**:135–142. doi:10.1038/nn.4195

Wimmer RD, Schmitt LI, Davidson TJ, Nakajima M, Deisseroth K, Halassa MM. 2015. Thalamic control of sensory selection in divided attention. *Nature* **526**:705–9. doi:10.1038/nature15398

983 Winn MB, Edwards JR, Litovsky RY. 2015. The Impact of Auditory Spectral Resolution on
984 Listening Effort Revealed by Pupil Dilation. *Ear Hear* **36**:e153–65.
985 doi:10.1097/AUD.0000000000000145
986 Woodruff PWR, Benson RR, Bandettini PA, Kwong KK, Howard RJ, Talavage T, Belliveau J,
987 Rosen BR. 1996. Modulation of auditory and visual cortex by selective attention is
988 modality-dependent. *Neuroreport Int J Rapid Commun Res Neurosci* **7**:1909–1913.
989 doi:10.1097/00001756-199608120-00007
990 Yin P, Fritz JB, Shamma SA. 2010. Do ferrets perceive relative pitch? *J Acoust Soc Am*
991 **127**:1673–1680.
992 Yin PP, Fritz JB, Shamma SA. 2014. Rapid spectrotemporal plasticity in primary auditory cortex
993 during behavior. *J Neurosci* **34**:4396–408. doi:10.1523/JNEUROSCI.2799-13.2014
994 Zekveld AA, Koelewijn T, Kramer SE. 2018. The Pupil Dilation Response to Auditory Stimuli:
995 Current State of Knowledge. SAGE Publications Inc. doi:10.1177/2331216518777174
996

Supplementary Figures

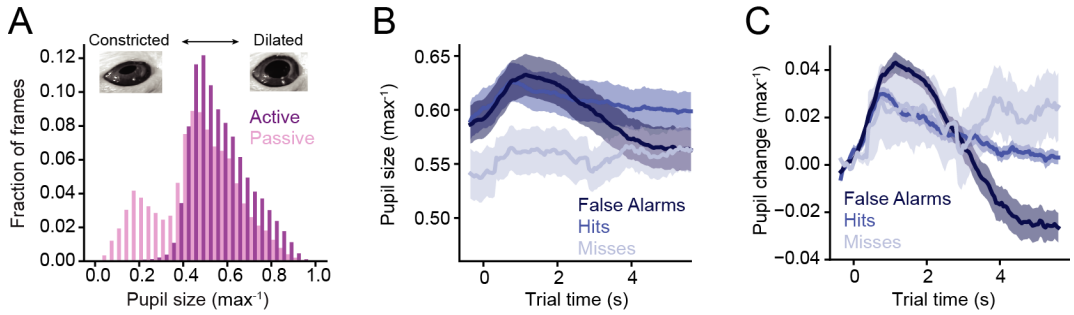

Figure S1: Pupil size correlates with task engagement and performance. **A.** Histogram of pupil size during passive and active blocks, averaged across all animals and physiological recording sessions. Pupil size is normalized to maximum per session. **B.** Mean timecourse of pupil size during behavior, grouped according to trial outcome (hit, miss, or false alarm). Mean pupil size was not significantly different for false alarm and hit trials ($p = 0.12$, sign test), but it was smaller during miss trials ($p = 0.0017$, sign test). Shading indicates SEM. **C.** Trial timecourse of average pupil change during active behavioral blocks and grouped according to performance, plotted as in B.

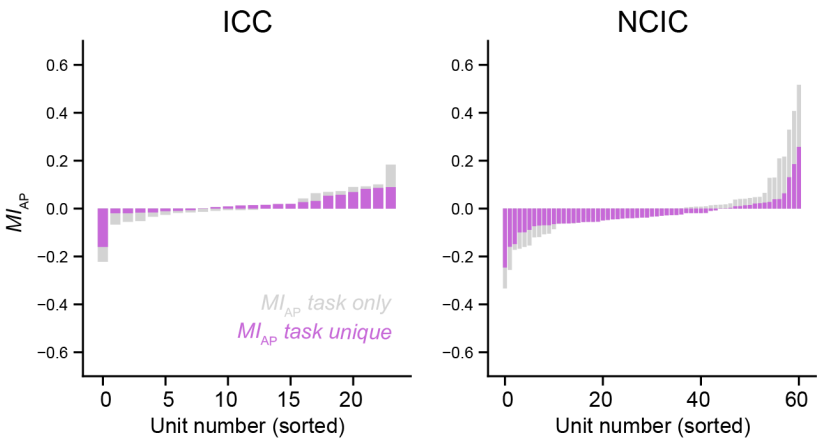

Figure S2: Task-related changes in central versus external inferior colliculus. Histograms of MI_{AP} *task-only* and MI_{AP} *task-unique* sorted according to their magnitude for each unit in ICC (left) and NCIC (right). The median magnitude of MI_{AP} *task-unique* was reduced by 43% relative to MI_{AP} *task-only* in ICC (Wilcoxon sign test: statistic = 57.0, p = 0.00788). Units in NCIC also showed a trend toward reduction, but the decrease was not significant (median decrease 31%, statistic = 865.0, p = 0.0563). Among ICC units with significant unique task modulation, n = 9/13 showed increased activity (MI_{AP} *task-unique* > 0) during behavior, and the median was not significantly different from zero (median 0.012, Wilcoxon signed rank test, statistic = 21.0, p = 0.08). Among NCIC units, only n = 8/36 were enhanced during behavior, and median was significantly less than zero (median -0.049, statistic = 118.0, p = 0.000731).

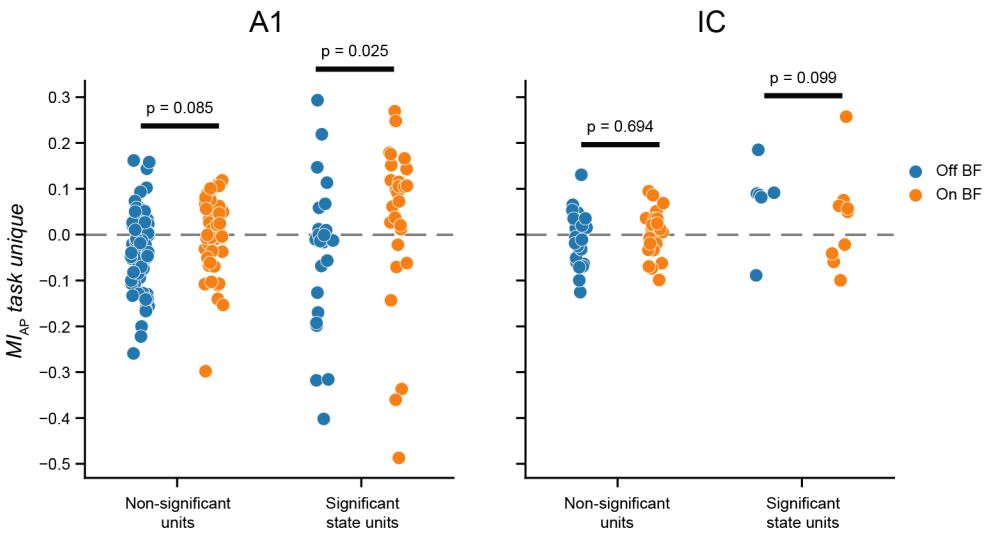

Figure S3: Frequency tuning versus task-related modulation of neural activity. Strip plots compare task-unique changes in activity (*MI_{AP} task-unique*) between units with best frequency similar to the target tone (on-BF, < 0.5 octave difference, blue) and different from the target tone (off-BF, > 0.5 octave difference, orange) in A1 (left) and IC (right). Data are further broken down by units with no task-unique changes (left) and significant changes ($p < 0.05$, permutation test, right). In A1, median *MI_{AP} task-unique* is significantly greater for modulated on-BF units (on-BF: median 0.082, $n = 28$; off-BF: -0.012, $n = 24$; $p = 0.025$, rank-sum test) but not for unmodulated units (on-BF: -0.002, $n = 44$; off-BF: -0.019, $n = 77$; $p = 0.085$). In IC, there are no differences between on- and off-BF units in the modulated (on-BF: median 0.05, $n = 9$; off-BF: 0.088, $n = 6$; $p = 0.099$, sign test) or unmodulated groups (on-BF: 0.006, $n = 25$; off-BF: 0.005, n=27; p=0.694). The relatively small number of significantly modulated IC units makes it difficult to interpret the absence of a significant on- versus off-BF difference, although it confirms that units with task-unique modulation are relatively rare in IC.

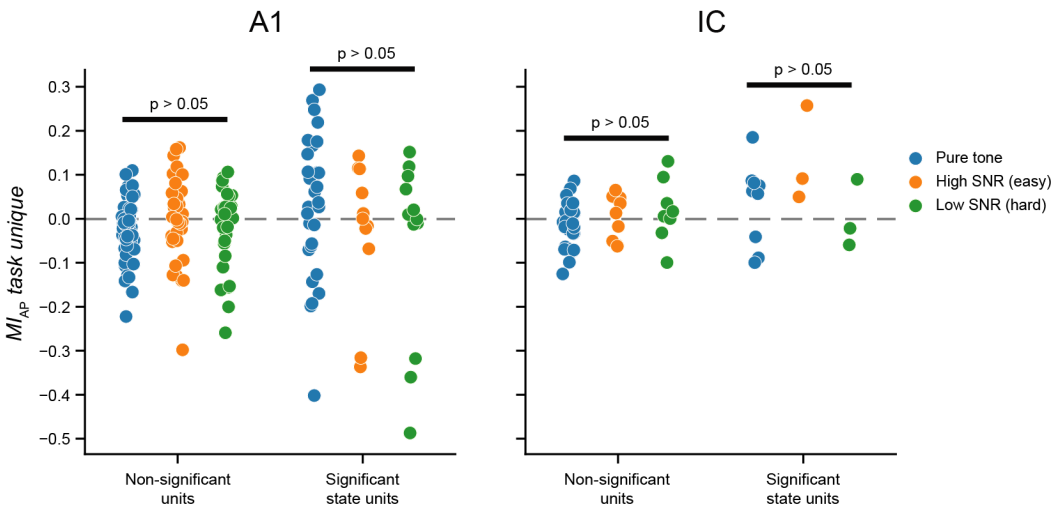

Figure S4: Task difficulty versus task-related modulation of neural activity. Swarm plots compare task-unique changes in activity (*MI_{AP} task-unique*) broken down by task difficulty, area (A1 or IC) and significance of task-unique modulation, plotted as in Figure S4. There is no difference in *MI_{AP} task-unique* between any pair of difficulty conditions in any group ($p > 0.05$, rank-sum test).

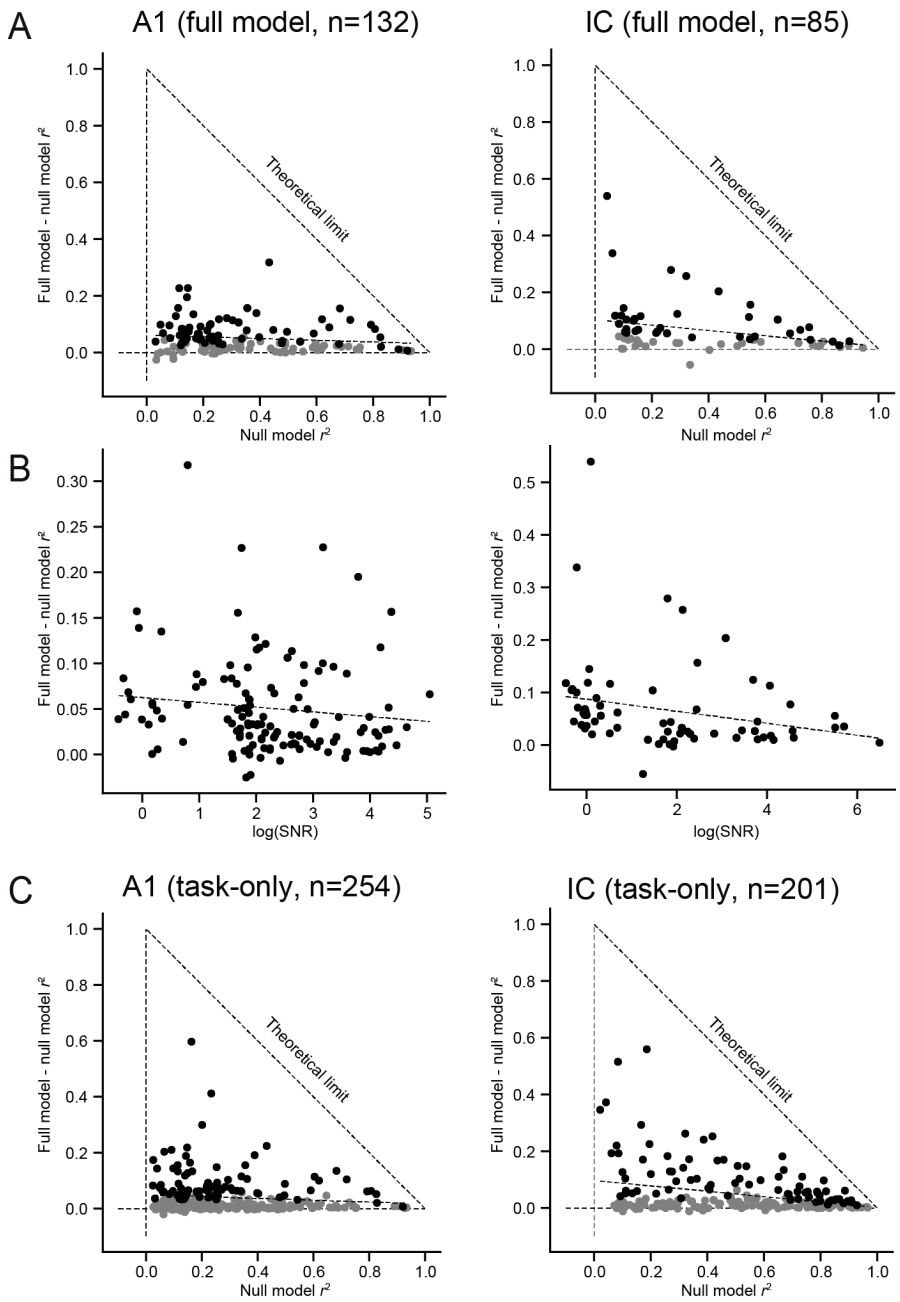

Figure S5: Auditory responsiveness predicts state-dependent modulation in IC. **A.** Scatter plots compare variance explained by the null model, a measure of auditory responsiveness for each neuron, against additional variance explained by the full model, which incorporates modulation by task engagement and arousal. In A1 (left), the additional variance explained by the full model is uncorrelated with null model performance (n = 132, r = -0.134, p = 0.125, Pearson's R). In IC,

the change is negatively correlated (IC: n = 85, r = -0.323 p = 0.00254), indicating a larger behavior effect in units with weaker auditory responses. Dashed diagonal line shows the theoretical limit on additional variance explained by the full model. If the additional variance explained is normalized by this limit, the data are positively correlated in A1 (r = 0.301, p = 4.61 x 10^{-4}) and not correlated in IC (r = 0.124, p = 0.258). **B.** Scatter plots compare log signal-to-noise ratio (SNR) of response evoked by reference noise-evoked, an alternative measure of auditory responsiveness, against additional variance explained by the full model. Again, there is no significant correlation in A1 (r=-0.121, p=0.165), but the correlation is negative in IC (r=-0.252, p=0.0202). **C.** Variance explained by the null model vs. additional variance explained by a behavior-dependent model for larger populations of neurons. Some data did not include pupillometry and the model accounted only for task engagement. Again, there was no correlation in A1 (n=254, r=-0.106, p=0.0910), but there is a negative correlation in IC (n=210, r=-0.317, p=2.78 x 10^{-6}).